HHS Public Access

Author manuscript

Nat Immunol. Author manuscript; available in PMC 2020 February 05.

Published in final edited form as:

Nat Immunol. 2019 September ; 20(9): 1208–1219. doi:10.1038/s41590-019-0442-x.

Functional Reprogramming of Regulatory T cells in the absence of Foxp3

Louis-Marie Charbonnier[1], **Ye Cui**[1], **Emmanuel Victor**[1], **Hani Harb**[1], **David Lopez**[2], **Jack J Bleesing**[3], **Maria I Garcia-Lloret**[4], **Karin Chen**[5], **Ahmet Ozen**[6], **Peter Carmeliet**[7], **Ming O Li**[8], **Matteo Pellegrini**[2], **Talal A Chatila**[1]

[1]Division of Immunology, Boston Children's Hospital, Department of Pediatrics, Harvard Medical School, Boston, MA 02115, U.S.A

[2]Department of Molecular, Cell and Developmental Biology, University of California, Los Angeles, CA 90095, U.S.A.

[3]Division of Bone Marrow Transplantation & Immune Deficiency, Cancer and Blood Diseases Institute, Cincinnati Children's Hospital Medical Center, Cincinnati, OH 45229

[4]Division of Allergy, Immunology, and Rheumatology, Department of Pediatrics, David Geffen School of Medicine at the University of California Los Angeles, Los Angeles, CA 90095

[5]Division of Allergy and Immunology, Department of Pediatrics, University of Utah School of Medicine, Salt Lake City, UT 84113

[6]Division of Pediatric Allergy/Immunology, Marmara University Faculty of Medicine, Istanbul, Turkey

[7]Laboratory of Angiogenesis and Vascular Metabolism, Center for Cancer Biology, VIB, KU Leuven, Campus Gasthuisberg O&N4, Herestraat 49-912, Leuven 3000, Belgium.

[8]Immunology Program, Memorial Sloan Kettering Cancer Center, New York, New York 10065, U.S.A.

Summary

Regulatory T cells (T_{reg} cells) deficient in the transcription factor Foxp3 lack suppressor function and manifest a T effector (T_{eff}) cell-like phenotype. We demonstrate that Foxp3 deficiency dysregulates metabolic checkpoint kinase mTORC2 signaling and gives rise to augmented aerobic glycolysis and oxidative phosphorylation. Specific deletion of the mTORC2 adaptor gene *Rictor* in Foxp3-deficient T_{reg} cells ameliorated disease in a *Foxo1* transcription factor-dependent manner. Rictor deficiency reestablished a subset of T_{reg} cell genetic circuits and suppressed the T_{eff} cell-

Correspondence should be addressed to T.A.C (talal.chatila@childrens.harvard.edu).

Author Contributions

L-M.C. and T.A.C. designed the experiments and evaluated the data; L-M.C., Y.C., E.V. H.H. and D.L. performed experiments; D.L. and M. P. performed gene expression profiling studies; J.J.B., M.I.G-L, K.C., A.O. M.O.L. and P.C. provided critical material. L-M.C. and T.A.C. conceived the project and directed the research; L-M.C. and T.A.C. wrote the manuscript.

Competing interests statement

The authors declare no competing interests.

like glycolytic and respiratory programs, which contributed to immune dysregulation. Treatment of T_{reg} cells from patients with FOXP3 deficiency with mTOR inhibitors similarly antagonized their T_{eff} cell-like program and restored suppressive function. Thus, regulatory function can be reestablished in Foxp3-deficient T_{reg} cells by targeting their metabolic pathways, providing opportunities to restore tolerance in T_{reg} cell disorders.

Introduction

Regulatory T cells (T_{reg} cells) enforce peripheral immunological tolerance by suppressing immune responses to self-antigens and innocuous environmental antigens [1, 2]. The Forkhead transcription factor Foxp3 is essential for T_{reg} cell differentiation and function [1, 3, 4]. While Foxp3 is not essential for thymic T_{reg} cell development, Foxp3-deficient T_{reg} cells (ΔT_{reg} cells) lack regulatory function [3, 4]. The core T_{reg} cell transcriptome and epigenome are largely preserved in ΔT_{reg} cells, although the expression of individual genes is frequently decreased [3, 4, 5]. Nevertheless, ΔT_{reg} cells acquire additional phenotypic and transcriptional attributes akin to those of effector T (T_{eff}) cell [3, 4, 6]. These findings led to the concept that Foxp3 stabilizes the transcriptome of T_{reg} cells and prevents their degeneration into T_{eff} cells [7].

T_{eff} cells undergo a profound change in their bioenergetic profile in favor of augmented aerobic glycolysis, oxidative phosphorylation (OXPHOS) and glutaminolysis as well as the de novo acquisition of biosynthetic pathways such as fatty acid synthesis [8]. T_{reg} cell metabolism is biased towards fatty acid oxidation (FAO) and pyruvate-dependent OXPHOS [9, 10, 11, 12], whereas glycolysis is kept under strict control. Enforced expression of Foxp3 promotes OXPHOS and suppresses glycolysis [13]. Reciprocally, upregulation of the glucose transporter Glut1 by toll-like receptor signaling, acting via the mammalian Target of Rapamycin Complex 1 (mTORC1), or by its enforced expression promoted T_{reg} cell proliferation but dampened Foxp3 expression and T_{reg} cell suppressive function [14]. We reasoned that interventions that deprive the T_{eff} cell-like programs of ΔT_{reg} cells of metabolic support may allow recovery of regulatory function by virtue of the preservation in those cells of a core regulatory transcriptome.

Results

Lineage-specific, Cre-mediated recombination in Foxp3-deficient T_{reg} cells

To enable genetic manipulations in ΔT_{reg} cells, we derived a bicistronic loss of function *Foxp3* allele, $Foxp3^{\Delta EGFPiCre}$, that contained a *Frt* element inserted between exons 9 and 10 that created an aberrant 3' splice junction site, leading to a premature stop codon in the *Foxp3* transcript. A ribosomal entry sequence inserted in the 3' untranslated region of *Foxp3* directed the expression of a humanized Cre recombinase (iCre) fused with the enhanced green fluorescent protein (EGFP) (Supplementary Fig. 1a–d). T_{reg} cells of $Foxp3^{\Delta EGFPiCre}$ mice expressed EGFP but not Foxp3 (Supplementary Fig. 1e, f). Analysis of $Foxp3^{\Delta EGFPiCre}$ mice harboring a Cre-inducible yellow fluorescent protein (YFP) transgene in the *Rosa26* locus ($R26^{YFP}$) revealed that all $EGFP^+$ cells were YFP^+ and virtually all within the $CD4^+$ T cell population (Supplementary Figure 1e). Comparison with wild-type mice carrying a

bacterial artificial chromosome (BAC) harboring a *Foxp3* promoter-driven EGFP and Cre recombinase and crossed with *R26*^{YFP} (*Foxp3*^{EGFPCre}*R26*^{YFP}) showed that the EGFP^{+} cells of *Foxp3*$^{\Delta EGFPiCre}$ mice were expanded, in agreement with previous studies on Foxp3-deficient mice (Supplementary Fig. 1e) [3, 4]. Within the YFP^{+} cell population, the frequency of cells that have downregulated their *Foxp3* locus activity (EGFP^{-}YFP^{+}) was modestly increased in the *Foxp3*$^{\Delta EGFPiCre}$*R26*^{YFP} males, pointing to incremental ΔT_{reg} cell instability.

Analysis of *Foxp3*^{EGFPCre} and *Foxp3*$^{\Delta EGFPiCre}$ EGFP^{-} and EGFP^{+} CD4^{+} T cells revealed that *Foxp3* transcripts were highly enriched in EGFP^{+} cells (Supplementary Fig. 1g). *Foxp3* transcripts were 20 fold higher in *Foxp3*^{EGFPCre} EGFP^{+} compared to *Foxp3*$^{\Delta EGFPiCre}$ EGFP^{+} cells, reflecting a positive feed-forward regulation by Foxp3 of its own gene expression (Supplementary Fig. 1g) [4]. EGFP^{+} ΔT_{reg} cells exhibited similar demethylation of the *Foxp3* CNS2 promoter region as EGFP^{+} control T_{reg} cells from *Foxp3*^{EGFP} knockin reporter allele mice, indicating that the ΔT_{reg} cells were epigenetically of T_{reg} cell lineage (Supplementary Fig. 1h).

Analysis of *Foxp3*$^{\Delta EGFPiCre/+}$ heterozygous females revealed that similar to the indigenous wild-type *Foxp3* allele, expression of *Foxp3*$^{\Delta EGFPiCre}$ in thymocytes was overwhelmingly restricted to the CD4^{+} lineage, starting at the CD4 single positive thymocyte stage (Supplementary Fig. 1i). However, the ΔT_{reg} cells were dramatically decreased in the periphery compared to wild-type T_{reg} cells, indicative of their reduced fitness (Supplementary Fig. 1i) [3, 4]. Overall, these results established that *Foxp3*$^{\Delta EGFPiCre}$ allele was specifically expressed in the T_{reg} cell lineage, and rendered these cells totally deficient in Foxp3 while enabling EGFP and Cre recombinase expression.

Inactivation of mTORC2 in ΔT_{reg} cells ameliorates disease

The mTOR pathways play a key role in promoting T_{eff} cell function [15, 16]. The mTOR kinase exists as part of two complexes: mTORC1 and mTORC2, that differentially contribute to T_H cell effector functions, while mTOR-deficient T cells differentiate in vitro into iT_{reg} cells [17, 18, 19]. mTORC1 acts as a finely-tuned T_{reg} cell metabolic checkpoint essential for T_{reg} cell homeostasis and function [20]. Activated mTORC1 phosphorylates the downstream substrates S6 and 4EBP, while activated mTORC2 phosphorylates the serine/threonine kinase AKT at serine residue 473 (p_{S473}AKT) [20, 21]. ΔT_{reg} cells from *Foxp3*$^{\Delta EGFPiCre}$ hemizygous mutant males, but not from heterozygous *Foxp3*$^{\Delta EGFPiCre/+}$ females, had increased pS6 and p4EBP at steady state compared to Foxp3-sufficient T_{reg} cells from *Foxp3*^{EGFPCre} mice (Fig. 1a,b and Supplementary Fig. 2a,b). However, both ΔT_{reg} cell populations upregulated their pS6 phosphorylation in response to anti-CD3 mAb stimulation to the same extent as Foxp3-sufficient T_{reg} cells, indicating that increased basal mTORC1 activity in male ΔT_{reg} cells was cell-extrinsic. Induction of p_{T308}AKT, a target of upstream Phosphoinositide-dependent kinase [22], was also increased to a similar extent in T_{reg} and ΔT_{reg} cells of *Foxp3*^{EGFPCre} and *Foxp3*$^{\Delta EGFPiCre}$ mice, respectively, upon anti-CD3 mAb stimulation (Supplementary Fig. 2a,b).

p_{S473}AKT was selectively increased in ΔT_{reg} cells of both hemizygous males and heterozygous females following anti-CD3 mAb stimulation, indicating that Foxp3 deficiency dysregulated mTORC2 activation in a cell intrinsic manner irrespective of the inflammatory

environment (Fig. 1a,b). The increased mTORC2 activity in ΔT_{reg} cells was associated with decreased protein expression of phosphatidylinositol-3,4,5-trisphosphate 3-phosphatase phosphatase and tensin homolog (PTEN) and PH-domain leucine-rich-repeat protein phosphatase 1 (PHLPP1), two phosphatases implicated in mTORC2 regulation [23, 24] (Supplementary Fig. 2c). We also evaluated proximal TCR signaling in ΔT_{reg} cells of *Foxp3*$^{\Delta EGFPiCre}$ mice by measuring Zeta-chain-associated protein kinase 70 (ZAP70) phosphorylation at tyrosine 319 residue upon anti-CD3 mAb stimulation, an event critical to downstream calcium mobilization, Ras activation and NFAT-dependent transcription [25]. ΔT_{reg} cells exhibited attenuated ZAP70 phosphorylation in response to anti-CD3 mAb stimulation compared to Foxp3-sufficient T_{reg} cells (Supplementary Fig. 2d). These results suggested that the enhanced mTORC2 activation in ΔT_{reg} cells of *Foxp3*$^{\Delta EGFPiCre}$ mice reflected impaired regulation by phosphatases.

Male mice hemizygous for the *Foxp3*$^{\Delta EGFPiCre}$ allele were runted and died early due to autoimmune lymphoproliferation, similar to another Foxp3-deficient mouse strain, *Foxp3*^{K276X}, that we previously generated [26] (Fig. 1c–f). We examined the role of dysregulated mTOR signaling in ΔT_{reg} cells of *Foxp3*$^{\Delta EGFPiCre}$ mice in their disease by cell-specific deletion of *Rptor* and *Rictor*, encoding the mTORC1 and mTORC2 regulators Raptor and Rictor, respectively. Expression of *Rptor* and *Rictor* transcripts was specifically abrogated in EGFP$^+$ cells of *Foxp3*$^{\Delta EGFPiCre}$*Rptor*$^{\Delta/\Delta}$ and *Foxp3*$^{\Delta EGFPiCre}$*Rictor*$^{\Delta/\Delta}$ mice, respectively (Supplementary Fig. 2e,f). Rictor protein expression was increased in EGFP$^+$ cells of *Foxp3*$^{\Delta EGFPiCre}$ mice, mirroring the increase in its transcripts, and was also abrogated in the ΔT_{reg} cells of *Foxp3*$^{\Delta EGFPiCre}$*Rictor*$^{\Delta/\Delta}$ mice, as confirmed by immunoblotting (Supplementary Fig. 2g). ΔT_{reg} cell-specific *Rictor* deletion markedly increased the body weight and survival of *Foxp3*$^{\Delta EGFPiCre}$ mice in a gene dose-dependent manner, whereas *Rptor* deletion did not (Fig. 1c,d). Furthermore, combined deletion of *Rictor* and *Rptor* in ΔT_{reg} cells of *Foxp3*$^{\Delta EGFPiCre}$*Rictor*$^{\Delta/\Delta}$*Rptor*$^{\Delta/\Delta}$ mice did not increase survival or body weight compared to *Foxp3*$^{\Delta EGFPiCre}$ or *Foxp3*$^{\Delta EGFPiCre}$*Rptor*$^{\Delta/\Delta}$ mice (Fig. 1c,d). *Foxp3*$^{\Delta EGFPiCre}$*Rictor*$^{\Delta/\Delta}$ mice had decreased tissue inflammation compared to *Foxp3*$^{\Delta EGFPiCre}$ mice but persistent lymphoproliferation (Fig. 1e–g).

The marked increase in ΔT_{reg} cells in *Foxp3*$^{\Delta EGFPiCre}$ mice was reversed in *Foxp3*$^{\Delta EGFPiCre}$*Rptor*$^{\Delta/\Delta}$ but not *Foxp3*$^{\Delta EGFPiCre}$*Rictor*$^{\Delta/\Delta}$ mice, indicating its dependence on mTORC1 activation (Supplementary Fig. 2h). The phenotype of EGFP$^+$ ΔT_{reg} cells of *Foxp3*$^{\Delta EGFPiCre}$ mice closely resembled that of ΔT_{reg} cells analyzed in earlier models [3, 4]. In addition to absent Foxp3 expression, ΔT_{reg} cells had lower expression of CD25 and CD73 and higher expression of ICOS, Helios, GITR, CD127, IL-2 and Granzyme B compared to WT T_{reg} cells (Supplementary Fig. 2i,j **and L-M.C., data not shown**). ΔT_{reg} cells of *Foxp3*$^{\Delta EGFPiCre}$*Rictor*$^{\Delta/\Delta}$ mice had upregulated expression of ICOS, Nrp1, GITR and CD73 compared to ΔT_{reg} cells from *Foxp3*$^{\Delta EGFPiCre}$ mice (Supplementary Fig. 2i,j). These results indicated that mTORC2 was specifically dysregulated in ΔT_{reg} cells in a cell-intrinsic manner, and promoted disease in Foxp3-deficient mice.

Rictor deficiency restores ΔT_{reg} cell suppressor function

Analysis of *Foxp3*$^{\Delta EGFPiCre}$*Rictor*$^{\Delta/\Delta}$ mice revealed that the frequencies of CD4 and CD8 effector memory cells were decreased by about 50% compared to *Foxp3*$^{\Delta EGFPiCre}$ mice, whereas those of naive and central memory T cells were increased (Fig. 2a,b and Supplementary Fig. 3a,b). Expression of the T_H1-associated transcription factor T-bet and IFN-γ was markedly increased in ΔT_{reg} and T_{eff} cells of *Foxp3*$^{\Delta EGFPiCre}$ *compared to* control *Foxp3*^{EGFPCre} mice, but was down-regulated by Rictor deficiency (*Foxp3*$^{\Delta EGFPiCre}$*Rictor*$^{\Delta/\Delta}$) By contrast, expression of the T_H2-associated transcription factor Gata-3 and IL-4, which was also increased in *Foxp3*$^{\Delta EGFPiCre}$ *Δ*T_{reg} and T_{eff} cells, was further upregulated in ΔT_{reg} cells by Rictor deficiency, thus confirming a critical role for mTORC2 in T_H1 but not T_H2 programming of ΔT_{reg} cells (Fig. 2a, b and Supplementary Fig. 3a,b). In contrast, expression of ROR-γt and IL-17 was unchanged (Supplementary Fig. 3a,b).

We next analyzed the impact of mTOR inhibition on T_{reg}, ΔT_{reg} and T_{eff} cell in vitro suppressive capacities. Pre-treatment of T_{eff} cells with the mTOR inhibitor Rapamycin did not confer them suppressive capacity. *Foxp3*$^{\Delta EGFPiCre}$ ΔT_{reg} cells had a small but detectable suppressive activity as compared to T_{eff} cells, which was augmented by Rapamycin pretreatment. Rapamycin pretreatment also enhanced the suppressive function of wild-type T_{reg} from *Foxp3*^{EGFPCre} (Fig. 2c).

The positive impact of rapamycin on ΔT_{reg} cell suppressive capacity mapped to mTORC2. *Rictor* deletion substantially upregulated ΔT_{reg} cell-mediated suppression (Fig. 2c), an effect that was not related to decreased ΔT_{reg} cell proliferation, as evidenced by Ki-67 staining (Supplementary Fig. 3a,b). Furthermore, Rictor but not Raptor deficiency abrogated the enhanced ΔT_{reg} cell suppressive activity mediated by Rapamycin, indicating that Rapamycin promoted ΔT_{reg} cell suppression by inhibiting mTORC2 (Fig. 2d,e).

We further compared the suppressive capacity of $CD4^+CD25^-$ T_{eff} cells isolated from *Cd4*^{Cre} versus *Cd4*^{Cre}*Rictor*$^{\Delta/\Delta}$ mice. Results showed that Rictor deficiency did not confer any suppressive capacity to T_{eff} cells. In contrast, Rictor deficiency in otherwise Foxp3-sufficient T_{reg} cells (*Foxp3*^{YFPCre}*Rictor*$^{\Delta/\Delta}$) resulted in a small but significant improvement in their suppressive capacity (Fig. 2f), consistent with the results of treating wild-type T_{reg} cells with Rapamycin (Fig. 2c).

The significance of improved wild-type T_{reg} cell function upon Rictor deficiency was evaluated *in vivo* using the lymphopenia colitis model [27]. *Foxp3*^{YFPCre}*Rictor*$^{\Delta/\Delta}$ T_{reg} cells proved superior in their capacity to control the intestinal inflammation in Rag1-deficient mice reconstituted with naive $CD4^+CD45RB^{high}$ T_{eff} cells. Under limiting T_{reg} cell availability (1:10 T_{reg}:T_{eff} cell ratio), the *Foxp3*^{YFPCre}*Rictor*$^{\Delta/\Delta}$ T_{reg} cells prevented weight loss, improved the intestinal inflammation and the inflammation-induced colon shortening, and suppressed the infiltration of the intestines by T_{eff} cells, including IFN-γ^+, IL-17^+ and IFN-γ^+IL-17^+ cells (Supplementary Fig. 4a–g).

We next analyzed the impact of *Rictor* deletion in ΔT_{reg} cells on their stability. Whereas ex-T_{reg} cells, corresponding to the $EGFP^-$ fraction of total YFP^+ CD4 T cells, represented

approximately 7% in Foxp3-sufficent control mice (*Foxp3*^{EGFPcre}*R26*^{YFP}) and 15% in Foxp3-deficient *Foxp3*$^{\Delta EGPiCre}$*R26*^{YFP} mice, their frequency was significantly decreased to 9–10% in *Foxp3*$^{\Delta EGFPiCre}$*Rictor*$^{\Delta/\Delta}$*R26*^{YFP} mice (Supplementary Fig. 3a,b), indicating that mTORC2 destabilized ΔT_{reg} cells, possibly by affecting their epigenetic demethylation [28].

We employed heterozygous *Foxp3*$^{\Delta EGFPiCre/+}$ female mice, which are phenotypically normal, to examine the impact of Rictor deficiency on ΔT_{reg} cells in the absence of systemic inflammation. ΔT_{reg} cells isolated from *Foxp3*$^{\Delta EGFPiCre/+}$ females had more suppressive activity at high $\Delta T_{reg}/T_{eff}$ cell ratios than those of *Foxp3*$^{\Delta EGFPiCre}$ males, indicative of a detrimental role for inflammation in the loss of ΔT_{reg} suppressive function (Fig. 3a). To assess T_{reg} cell fitness, we examined the frequencies of wild-type and ΔT_{reg} cells in *Foxp3*$^{\Delta EGFPiCre/+}$*R26*^{YFP} versus *Foxp3*$^{\Delta EGFPiCre/+}$*Rictor*$^{\Delta/\Delta}$*R26*^{YFP} heterozygous female mice. Whereas ΔT_{reg} cells were profoundly under-represented in *Foxp3*$^{\Delta EGFPiCre/+}$ mice compared to T_{reg} cells carrying the wild-type *Foxp3* allele, their frequency increased in *Foxp3*$^{\Delta EGFPiCre/+}$*Rictor*$^{\Delta/\Delta}$*R26*^{YFP} mice, indicative of their improved fitness (Fig. 3b,c). ΔT_{reg} cells from *Foxp3*$^{\Delta EGFPiCre/+}$*R26*^{YFP} and *Foxp3*$^{\Delta EGFPiCre/+}$*Rictor*$^{\Delta/\Delta}$*R26*^{YFP} heterozygous females minimally expressed T-bet/IFN-γ and Gata-3/IL-4 compared to ΔT_{reg} cells of hemizygous males Fig. 3d,e). These results indicate that the acquisition by ΔT_{reg} cells of T_H cell-like phenotypes was augmented by the intense inflammatory environment in Foxp3-deficient males. Further characterization of ΔT_{reg} cells of *Foxp3*$^{\Delta EGFPiCre/+}$*R26*^{YFP} and *Foxp3*$^{\Delta EGFPiCre/+}$*Rictor*$^{\Delta/\Delta}$*R26*^{YFP} heterozygous females revealed increased expression of CD25 and Nrp1 in Rictor-deficient ΔT_{reg} cells (Fig. 3f). Overall, the results in Fig. 2 and Fig. 3 show that mTORC2 was cell intrinsically dysregulated in ΔT_{reg} cells, and that its inhibition substantially restored ΔT_{reg} cell function.

mTORC2 dependent and independent transcriptional programs in ΔT_{reg} cells

We compared the transcriptomes of ΔT_{reg} and T_{reg} isolated from female mice that carried one mutant *Foxp3*$^{\Delta EGFPiCre}$ allele and a second competent *Foxp3* allele (*Foxp3*^{RFP}) that also directed the expression of the red fluorescent protein (RFP), thus allowing for color sorting of the respective populations [29]. We extended these studies to examine the transcriptome of ΔT_{reg} cells of *Foxp3*$^{\Delta EGFPiCre/+}$*Rictor*$^{\Delta/\Delta}$ females to identify transcriptional pathways altered by *Rictor*. Results revealed global changes in the transcriptional landscape induced by Foxp3 deficiency. Concurrent Rictor deficiency normalized some of these changes, while also inducing *de novo* Foxp3-independent transcriptional alterations of its own Fig. 4a,b and Data Set 1). ΔT_{reg} cells exhibited decreased expression of some genes associated with the T_{reg} cell transcriptome (e.g. *Itgae*, *Fgl2*, *Nrp1*, *Ebi3a*, *Il2ra*, *Ikzf2*, *Tigit*) and the acquisition of several others associated with T_{eff} cells, including T_H17 cells (e.g. *Rorc*, *Tgfb3*, *Il17a*, *Nr1d1*, *Sgk1*), cytokines and cellular activators (*Il2*, *Il21, Cd40lg*).

Relevant to the mTOR pathway, ΔT_{reg} cells had increased expression of *Prr5l*, encoding an mTORC2 regulator that directs its substrate specificity [30], and decreased expression of *Phlpp1*, encoding the phosphatase PHLPP1 [23]. Concurrent Rictor deficiency upregulated a subset of the core T_{reg} transcriptome genes, including *Fgl2, Il10*, *Lag3*, *Tnfrsf18* (*Gitr*), *Ebi3*, *Nrp1*, *Il2ra*, *Ctla4* and *Nt5e*. It also down-regulated the expression of genes associated with the T_H17 (*Rorc*, *Tgfb3*) and T follicular helper cell (*Cxcr5* and *Bcl6)* lineages, while

upregulating the *Bcl6* antagonist *Prdm1* Fig. 4c,d and Data Set 2). These results suggested that Rictor deficiency altered the ΔT_{reg} cell transcriptome in favor of improved regulatory function.

Of particular interest was the role of increased IL-10 and Blimp1 expression in Rictor-deficient ΔT_{reg} cells (Fig. 4e). Blimp1 binds to the regulatory CNS –9 element located proximal to the *Il10* gene to promote *Il0* transcription [31]. Chromatin immunoprecipitation (ChIP) studies demonstrated increased binding of Blimp1 to the *Il10* CNS–9 element of Rictor-deficient ΔT_{reg} cells (Fig. 4f). IL-10 neutralization largely abrogated the improved *in vitro* suppressive capacity of Rictor deficient ΔT_{reg} cells, indicating a mechanistic role for this pathway in their augmented regulator function (Fig. 4g).

mTORC2 signaling in ΔT_{reg} cells activates the AKT-FOXO1 axis

We examined mTORC2 activity, as monitored by p_{S473}AKT staining, in wild-type T_{reg} cells from *Foxp3*^{EGFP} mice, and in ΔT_{reg} cells from *Foxp3*$^{\Delta EGFPiCre}$ and *Foxp3*$^{\Delta EGFPiCre}$*Rictor*$^{\Delta/\Delta}$ mice. The increase in p_{S473}AKT staining in *Foxp3*$^{\Delta EGFPiCre}$ ΔT_{reg} cells following their stimulation with anti-CD3+anti-CD28 mAbs was totally reversed in the *Foxp3*$^{\Delta EGFPiCre}$*Rictor*$^{\Delta/\Delta}$ ΔT_{reg} cells Fig. 5a,b). AKT phosphorylates the transcription factor Foxo1, resulting in its retention in the cytosol and its ubiquitination and degradation [32]. Foxo1 in turn negatively regulates T_H1 differentiation of T_{reg} cells by suppressing the transcription of *Ifng* and other T_H1 genes [33, 34]. Expression of several Foxo1-regulated genes, including *Il7r*, *Cd55*, *Cd83*, *Emb*, *Etv5* and *Mafg*, was affected in *Foxp3*$^{\Delta EGFPiCre}$ ΔT_{reg} cells and normalized in *Foxp3*$^{\Delta EGFPiCre}$*Rictor*$^{\Delta/\Delta}$ ΔT_{reg} cells (Data Set 2). Foxo1 was decreased in the nucleus in anti-CD3 mAb-stimulated ΔT_{reg} cells of *Foxp3*$^{\Delta EGFPiCre}$ compared to control *Foxp3*^{EGFP} T_{reg} cells, a deficit that was reversed in *Foxp3*$^{\Delta EGFPiCre}$*Rictor*$^{\Delta/\Delta}$ ΔT_{reg} cells Fig. 5c,d). Also, *Rictor* deletion increased Foxo1 binding at the *Ifng* and *Tbx21* promoters (Fig. 4g).

We examined the consequences of deleting a floxed *Foxo1* gene in *Foxp3*$^{\Delta EGFPiCre}$*Rictor*$^{\Delta/\Delta}$ ΔT_{reg} cells. The triple mutant *Foxp3*$^{\Delta EGFPiCre}$*Rictor*$^{\Delta/\Delta}$*Foxo1*$^{\Delta/\Delta}$ mice were similar to single mutant *Foxp3*$^{\Delta EGFPiCre}$ and the double mutant *Foxp3*$^{\Delta EGFPiCre}$*Foxo1*$^{\Delta/\Delta}$ mice in terms of growth and survival, dysregulated T_{eff} cells and IFN-γ expression in both ΔT_{reg} and T_{eff} cells, whereas the IL-4 response was unaffected Fig. 5e,f and Supplementary Fig. 5a–e). *Foxo1* deletion reversed the upregulation of *Il10* expression in *Foxp3*$^{\Delta EGFPiCre}$*Rictor*$^{\Delta/\Delta}$ ΔT_{reg} (Supplementary Fig. 5f). Reciprocally, ΔT_{reg} cell-specific expression of Cre-regulated AKT-insensitive *Foxo1* transgene (*R26*^{Foxo1AAA}) partially recapitulated the effects of Rictor deficiency in improving weight gain, prolonging survival and augmenting ΔTreg cell suppressive capacity (Supplementary Fig. 5a–d) [33]. It also down-regulated T_{eff} cell activation and the T_H1 programming of ΔT_{reg} cells Fig. 5e,f and Supplementary Fig. 5e,g). These results indicated that the effects of Rictor deletion in promoting ΔT_{reg} cell function largely proceeded by Foxo1-dependent mechanisms.

Rictor deficiency resets the metabolism of ΔT_{reg} cells

Dysregulation of the mTORC2-Foxo1 axis upregulates glycolysis and OXPHOS [35, 36]. T_{reg} cells and naive T cells exhibit low levels of glycolysis in favor of increased OXPHOS,

whereas T_{eff} cells manifest increased aerobic glycolysis, products of which feed into DNA and protein synthesis [37]. *Foxp3*$^{\Delta EGFPiCre}$ ΔT_{reg} cells had increased expression of several enzymes in the glycolytic and pentose phosphate shunt pathways, several of which were reset back to baseline upon concurrent Rictor deficiency (e.g. *Gpi*, *Aldoa*, *Eno1*, *Pkm2* and the pentose phosphate shunt enzymes) (Supplementary Fig. 6a). Some glycolytic enzymes were down-regulated by Rictor deficiency but remained increased above their levels in wild-type T_{reg} cells (e.g. *Hk2*, *Gapdh*), while others such as *Tpi* and the glycolytic regulator *Pfkfb3*, which were upregulated in Foxp3-deficient T_{reg} cells, were either unaffected or further upregulated by Rictor deficiency.

Unlike wild-type T_{reg} cells, *Foxp3*$^{\Delta EGFPiCre}$ ΔT_{reg} cells stimulated with anti-CD3 mAb and IL-2 exhibited exaggerated lactate production similar to activated T_{eff} cells, which was markedly reduced in *Foxp3*$^{\Delta EGFPiCre}$*Rictor*$^{\Delta/\Delta}$ ΔT_{reg} cells (Supplementary Fig. 6b). Glycolysis and OXPHOS were further evaluated in *Foxp3*^{EGFP} (wild-type) T_{reg} cells and *Foxp3*$^{\Delta EGFPiCre}$ and *Foxp3*$^{\Delta EGFPiCre}$*Rictor*$^{\Delta/\Delta}$ ΔT_{reg} cells isolated from hemizygous males using an extracellular metabolic flux analyzer. Of the three T_{reg} cell populations, *Foxp3*$^{\Delta EGFPiCre}$ ΔT_{reg} cells exhibited the largest increase in extracellular acidification rate (ECAR), a measure of glycolysis, upon D-glucose supplementation, while *Foxp3*$^{\Delta EGFPiCre}$*Rictor*$^{\Delta/\Delta}$ ΔT_{reg} had an intermediate phenotype Fig. 6a,b). All three T_{reg} cells populations exhibited a modest drop in ECAR upon Oligomycin supplementation, indicating that glycolysis had peaked following glucose addition [38].

OXPHOS, as assessed by the oxygen consumption rate (OCR), was also markedly increased in *Foxp3*$^{\Delta EGFPiCre}$ ΔT_{reg} cells. Both basal respiration, ATP-coupled respiration and respiratory reserve were increased in *Foxp3*$^{\Delta EGFPiCre}$ ΔT_{reg} compared to control T_{reg} cells whereas *Foxp3*$^{\Delta EGFPiCre}$*Rictor*$^{\Delta/\Delta}$ ΔT_{reg} had an intermediate phenotype.. Fig. 6a,b).

The ECAR and OCR of ΔT_{reg} cells of *Foxp3*$^{\Delta EGFPiCre/+}$ females were also highly increased, indicative of cell-intrinsic metabolic changes (Supplementary Fig. 6c,d). Rictor deficiency completely reversed the increase in ECAR in ΔT_{reg} cells of *Foxp3*$^{\Delta EGFPiCre/+}$ females, but only partially reversed the increase in OCR, indicating that additional pathways contributed to the latter's dysregulation (Supplementary Fig. 6c,d).

The contribution of inputs from glycolysis, glutaminolysis and FAO to the OCR was measured upon the sequential addition of specific metabolic inhibitors: UK5099 for glycolysis, Etomoxir for FAO and BTPES for glutaminolysis (Fig. 6c). Whereas the OCR in wild-type T_{reg} cells is fatty acid-dependent, it becomes glucose- and to a lesser extent glutamate-dependent in *Foxp3*$^{\Delta EGFPiCre}$ ΔT_{reg} cells, pointing to a shift from FAO to aerobic glycolysis and, secondarily, glutaminolysis (Fig. 6c). Rictor deficiency reduced the OCR and decreased aerobic glycolysis Fig. 6c). Transcripts of key factors associated with aerobic glycolysis, including *Myc* and *Hif1a* [12, 39], were markedly increased in *Foxp3*$^{\Delta EGFPiCre}$ ΔT_{reg} cells, and partially corrected in *Foxp3*$^{\Delta EGFPiCre}$*Rictor*$^{\Delta/\Delta}$ ΔT_{reg} cells (Supplementary Fig. 6e).

Metabolomic analysis on *Foxp3*$^{\Delta EGFPiCre}$ and *Foxp3*$^{\Delta EGFPiCre}$*Rictor*$^{\Delta/\Delta}$ ΔT_{reg} cells, and control T_{reg} and T_{eff} cells from *Foxp3*^{EGFP} mice revealed increased glycolytic

(phosphoenolpyruvate, lactate) and citric acid cycle (fumarate, malate) metabolites in *Foxp3*$^{\Delta EGFPiCre}$ ΔT_{reg} cells, which were reversed in *Foxp3*$^{\Delta EGFPiCre}$*Rictor*$^{\Delta/\Delta}$ ΔT_{reg} cells Fig. 6d and Supplementary Fig. 6f). *Foxp3*$^{\Delta EGFPiCre}$ ΔT_{reg} cells were deficient in carnitine, necessary for the transport of fatty acids to the mitochondria for beta oxidation, which was not corrected by Rictor deficiency Fig. 6d and Supplementary Fig. 6f) [40]. These results established that *Foxp3*$^{\Delta EGFPiCre}$ ΔT_{reg} cells exhibited robust mTORC2-dependent aerobic glycolysis and OXPHOS.

Metabolic blockade inhibits the T_{eff}-like phenotype of ΔT_{reg} cells

The role of dysregulated glycolysis in ΔT_{reg} cell dysfunction was probed by cell-specific deletion of *Pfkfb3*, encoding 6-Phosphofructo-2-Kinase/Fructose-2,6-Biphosphatase 3. This enzyme synthesizes fructose-2,6-bisphosphate, an allosteric activator of phosphofructokinase-1 and a powerful stimulator of glycolysis [41]. ΔT_{reg} cell-specific deletion of *Pfkfb3* (*Foxp3*$^{\Delta EGFPiCre}$*Pfkfb3*$^{\Delta/\Delta}$) normalized their ECAR, while minimally impacting the OCR (Fig. 7a). *Foxp3*$^{\Delta EGFPiCre}$*Pfkfb3*$^{\Delta/\Delta}$ mice showed decreased memory T_{eff} cells, at values intermediate between *Foxp3*$^{\Delta EGFPiCre}$ and *Foxp3*$^{\Delta EGFPiCre}$*Rictor*$^{\Delta/\Delta}$ mice (Fig. 7b). ΔT_{reg} cell-specific PFKFB3 deficiency suppressed IFN-γ production by ΔT_{reg} and T_{eff} cells, whereas IL-4 production was not affected. Concurrent deletion of *Pfkfb3* and *Rictor* were not additive, indicating that effects of PFKFB3 deficiency on glycolysis were subsumed under mTORC2 deficiency (Fig. 7b). PFKFB3 deficiency marginally improved *in vitro* ΔT_{reg} cells suppression of T_{eff} cell proliferation (Fig. 7c), Thus, the inhibition of dysregulated glycolysis by *Rictor* or *Pfkfb3* deletion restored ΔT_{reg} cells regulation of T_H1 cell responses.

We further investigated the dysregulated metabolism of ΔT_{reg} cell using 2-deoxyglucose (2DG), a competitive inhibitor of glycolysis. While *Pfkfb3* deletion attenuated the ECAR in ΔT_{reg} cells, 2DG more profoundly suppressed it (Fig. 6a). 2DG strongly inhibited the production by *Foxp3*$^{\Delta EGFPiCre}$ and *Foxp3*$^{\Delta EGFPiCre}$*Rictor*$^{\Delta/\Delta}$ ΔT_{reg} cells of both of IFN-γ and IL-4 (Fig. 7d), and at high concentrations partially restored *Foxp3*$^{\Delta EGFPiCre}$ ΔT_{reg} cell suppression, suggesting a role for aerobic glycolysis-dependent T_H cytokine production in poor ΔT_{reg} cell suppression (Fig. 7e).

In vivo, treatment of *Foxp3*$^{\Delta EGFiCre}$*R26*^{YFP} mice with 2DG resulted in decreased tissue inflammation Fig. 7f–h). 2DG reduced the frequencies of memory CD62L^{lo}CD44^{hi} CD4$^+$ and CD8$^+$ T cells, and the production of IL-4 and IFN-γ and the expression of Gata-3 and T-bet expression by both CD4$^+$ T_{eff} and T_{reg} cells. 2DG treatment of *Foxp3*$^{\Delta EGFPiCre}$*Rictor*$^{\Delta/\Delta}$ mice also reduced the memory frequencies and cytokine production by CD4$^+$ and CD8$^+$ T cells (Supplementary Fig. 7).

mTOR inhibition upregulates human mutant FOXP3 T_{reg} cell suppressive function

FOXP3 deficiency causes a human autoimmune lymphoproliferative disease, Immune dysregulation, Enteropathy, Polyendocrinopathy X-Linked or IPEX [42]. Similar to ΔT_{reg} cells, IPEX T_{reg} cells are present in the periphery but are deficient in suppressive functions [43, 44]. We analyzed T_{reg} cells of five IPEX patients with different *FOXP3* mutations, including N-terminal (C169Y), linker region (R309N) and forkhead domain (A384T and

N388S) missense mutations and an inactivating mutation in the 3' polyadenylation signal (Fig. 8a). The C169Y, R309N and N388S are novel mutations, while the A384T and the 3' polyadenylation signal mutation have been reported [45]. All five IPEX patients exhibited detectable but lower expression of FOXP3 in their mutant T_{reg} cells, defined as $CD4^+CD25^+CD127^{lo}$ [46, 47], compared to control subject T_{reg} cells (Supplementary Figure 8). There was a similar increase in pS6 phosphorylation in control and IPEX T_{reg} cells in response to cell activation, which was abrogated by treatment with the dual mTOR inhibitor Ku-0063794 (Fig 8b). By contrast, increased p_{S473}AKT phosphorylation was exclusively observed in stimulated IPEX T_{reg} cells, which was also abrogated by the inhibitor (Fig 8c). Thus, mTORC2 activity was also dysregulated in IPEX T_{reg} cells.

Examination of metabolic activities revealed that IPEX T_{reg} cells exhibited increased ECAR in response to D-glucose, indicative of heightened glycolytic function, while showing equivalent glycolytic reserves following oligomycin addition (Fig. 8d). Both glycolytic components were inhibited by treatment of T_{reg} cells with the dual mTOR inhibitor. IPEX T_{reg} cells also exhibited exaggerated OCR responses, which were also inhibited by treatment with the dual mTOR inhibitor (Fig. 8e).

While control T_{reg} cells effectively suppressed T_{eff} cell proliferation, IPEX T_{reg} cells did not Fig. 8f,g). Pretreatment of the latter with the dual mTOR inhibitor uniformly improved their suppressor function irrespective of the underlying mutation involved Fig. 8f,g). mTOR inhibition also upregulated the suppressive function of T_{reg} cells of healthy subjects Fig. 8g), similar to Foxp3-sufficient but Rictor-deficient mouse T_{reg} cells (Fig. 2f and Supplementary Fig. 4). IPEX T_{reg} cells expressed both IFN-γ and IL-4, indicative of their T_{eff}-like phenotype. mTOR inhibition suppressed the T_H1 but not the T_H2 response, reflecting the role of mTORC2 in driving the T_H1 response in ΔT_{reg} cells (Fig. 8h). These results support the targeting of mTOR pathways to restore T_{reg} cell function in IPEX, as well as augmenting Foxp3-sufficient T_{reg} cell function in immune dysregulatory diseases.

Discussion

We demonstrate that the skewing of T_{reg} cells towards a T_{eff} cell-like phenotype upon Foxp3 deficiency is critically dependent on a limited set of molecular pathways, including mTORC2 and glycolysis. Furthermore, inhibition of these pathways specifically in Foxp3-deficient T_{reg} cells partially restored regulatory function and attenuated disease. Targeting the same pathways may also improve the stability and function of Foxp3-sufficient T_{reg} cells in inflammatory and autoimmune diseases.

Our studies implicated impaired regulation by phosphatases, including PTEN and PHLPP1, in mTORC2 dysregulation in ΔT_{reg} cells. *Pten* deletion dysregulates mTORC2 and results in the loss of T_{reg} cell regulatory function [38]. PTEN and AKT phosphatase PHLPP1 were markedly decreased in ΔT_{reg} cells, while transcripts encoding both Rictor and the Rictor-associated protein PRR5L, which regulates mTORC2 activity in a substrate-specific manner [30], were increased. Collectively, these abnormalities may favor heightened mTORC2 activity.

The mechanisms by which mTORC2 dysregulation impair ΔT_{reg} cell regulatory functions included disruption of Blimp1 and Foxo1-dependent induction of IL-10 [31, 48]. The salutary effects of Rictor deficiency on ΔT_{reg} cells were were reversed by Foxo1 deficiency. Reciprocally expression of a *Foxo1* gain-of-function mutant transgene recapitulated the effects of Rictor deficiency, rendering ΔT_{reg} cells less T_H1 cell-like, consistent with the role of Foxo1 in suppressing T_{reg} cells T_H1 reprogramming [33].

The relationship of the metabolic resetting induced by Rictor deletion with enhanced ΔT_{reg} cell function was further established using pharmacological and genetic approaches, including inhibition of aerobic glycolysis with 2-DG and ΔT_{reg} cell-specific deletion of *Pfkfb3*. Rictor deficiency did not attenuate the T_H2 program in ΔT_{reg} cells and in fact exacerbated it, an effect not observed upon glycolytic pathway inhibition with 2DG treatment or *Pfkfb3* deletion. These results suggest that the T_H2 cell program in ΔT_{reg} cells is regulated by mTORC2 by distinct mechanisms(s)

Unlike ΔT_{reg} cells of *Foxp3*$^{\Delta EGFPiCre}$ hemizygous male mice, those of *Foxp3*$^{\Delta EGFPiCre/+}$ heterozygous females manifested residual suppressive activity and did not express T_H cell cytokines, indicating that the intense inflammatory environment of mutant male mice further contributed to the T_{eff} cell-like phenotype of ΔT_{reg} cells. These findings suggested that suppression of systemic immune activation may act in an adjunct manner with mTORC2 inhibition to further antagonize the T_{eff} cell-like phenotype of ΔT_{reg} cells and to promote their regulatory function.

IPEX-causing *FOXP3* mutations may completely inactivate FOXP3 or more selectively impair its functions [45]. Studies on mice harboring IPEX-causing *FOXP3* mutations, including I363V, A384T and R397W, have identified divergent mechanisms by which these mutations impair Foxp3 function [49, 50]. Common to these mutations is the acquisition by the T_{reg} cells of T_{eff} cell-like attributes, with the impaired regulatory function [49]. IPEX T_{reg} cells also responded favorably to mTOR inhibitors, with decreased cytokine expression and improved suppression, indicating that targeting mTORC2 is a viable therapeutic strategy in this disorder. More broadly, our studies open up the possibility of combinatorial interventions that target distinct metabolic pathways in T_{reg} cells to restore immune tolerance in a variety of immune dysregulatory diseases.

Methods

Human subjects

Male subjects with IPEX-causing *FOXP3* mutations and healthy controls were recruited under protocols approved by the local Institutional Review Boards at the respective referring centers. Patient P1, P2, P3 and P4 each harbored a missense mutation at c.505G>A (p.C169Y), c.926G>A (p.R309N), c.1150G>A (p.A384T), c.1163A>G (p.N388S) respectively (reference sequence NM_014009.3). Patient P5 suffered from a previously described inactivating mutation in the *FOXP3* 3' polyadenylation signal [51].

Generation of *Foxp3*$^{\Delta EGFPiCre}$ mice

Foxp3 genomic DNA was isolated from a bacterial artificial chromosome clone (Genome Systems) and subcloned into the plasmid vector pKO (Lexicon). A DNA cassette encoding for an improved Cre recombinase (iCre) was isolated from the paavCAG-iCre plasmid (Addgene) and inserted at the BSGRI site of a pIRES2-EGFP (Addgene) vector containing a DNA cassette composed of an internal ribosomal entry sequence (IRES) linked to downstream EGFP and SV40 poly-A sequences. The IRES-EGFP-iCre sequence was inserted by blunt-end ligation at the SSPI restriction site immediately downstream of the Foxp3 translational stop codon and upstream of the endogenous polyadenylation signal. A *PGK*-neo cassette was also inserted at the EcoRI site in intron 9 of Foxp3 in the opposite orientation of Foxp3 and was flanked by two FRT sites to allow excision by FLP-mediated recombination. The targeting construct also included a diphtheria toxin gene (DT) for negative selection against randomly inserted targeting constructs.

Targeting plasmids were introduced by electroporation into SCC10 embryonic stem cells and subjected to G418 selection. Resistant clones were screened by Southern blot. Successfully targeted clones were injected into C57BL/6 blastocysts, and chimeric males were mated with Wild-type (WT) C57/BL6/J females to derive N1 females that have transmitted the bicistronic allele together with the PGK-neo cassette insert (*Foxp3*$^{EGFPiCre\text{-}neo}$) in the germline. The PGK-neo cassette was removed by mating founder males with Flp-deleter female mice that harbor a constitutive, ubiquitously expressed *FLP* recombinase allele [52]. Male offspring hemizygous for *Foxp3*$^{\Delta EGFPiCre}$ allele (minus the PGK-neo cassette) presented Scurfy phenotype. The PCR products of Exon9/Exon10 obtained using complementary and genomic DNA (cDNA and gDNA, respectively) were amplified by the following primer sequences: *Foxp3* Exon9 Forward 5'-CTTCCACAACATGGACTACTTCAA-3' and *Foxp3* Exon10 Reverse 5'-AAGTAGGCGAACATGCGAGT-3'. The PCR product obtained from gDNA was purified and sequenced by Sanger sequencing using *Foxp3* Exon9 Forward primer.

Mice

Foxp3^{EGFPCre}, *Foxp3*^{YFPCre}, *CD4*^{Cre}, *Rptor*$^{fl/fl}$, *Foxo1*$^{fl/fl}$, *R26*^{YFP} and *Rag1*$^{-/-}$ mice were obtained from the Jackson Laboratory. *Rictor*$^{fl/fl}$ mice were obtained from the Mutant Mouse Regional Resource Center. *R26*^{Foxo1AAA} and *Pfkfb3*$^{fl/fl}$ mice were generated as described [33, 41]. *Foxp3*^{K276X}, *Foxp3*^{EGFP}, *CD45.1 Foxp3*^{EGFP}, *Foxp3*$^{\Delta EGFPiCre}$ and their respective crosses were backcrossed 8–10 generations on C57BL/6J, excepted *Foxp3*$^{\Delta EGFPiCre}$*Foxo1*$^{\Delta/\Delta}$ and *Foxp3*$^{\Delta EGFPiCre}$*Rictor*$^{\Delta/\Delta}$*Foxo1*$^{\Delta/\Delta}$ strain. A list of all mouse strains used is reported in Supplementary Table 1. Excepted when it was specified, 25–28 days old mice were used in this study. The mice were housed under specific pathogen-free conditions and used according to the guidelines of the institutional Animal Research Committees at the Boston Children's Hospital.

Real-time PCR

Total RNA was isolated from sorted cells with RNeasy kit (Qiagen). Reverse transcription was performed with the SuperScript II RT-PCR system (Invitrogen) and quantitative real-time reverse transcription (RT)-PCR with Taqman® Fast Universal PCR master mix, internal

house-keeping gene mouse (*Actin* VIC-MGB dye) and specific target gene primers (FAM Dye) (Applied Biosystems) on Step-One-Plus machine. Relative expression was normalized to Actin for genes encoding for the enzymes of the glycolysis cascade (*Scl2a3, Hk1, Hk2*, *Gpi*, *Pfkfb3*, *Aldoa*, *Gapdh, Tpi*, *Pdk1, Pgam1*, *Pgam5*, *Eno1, Pkm2, Ldha*, *Scl16a1*), the pentose phosphate cycle (*G6pdx*, *Pgd*, *Rpia*, *Rpe*), *Foxp3*, *Rictor*, *Rptor, HIF1a and Myc* and calculated as fold change compared to WT $CD4^+GFP^-$ T_{eff} cells or WT $CD4^+GFP^-$ T_{reg} cells isolated from $Foxp3^{EGFP}$ mice.

Flow cytometry

Viability dye and antibodies against mouse CD4, CD8, CD16/CD32, CD90.2, CTLA4, ICOS, CD73, Blimp-1 (biolegend), CD25, CD44, CD45.1, CD45.2, CD62L, Foxp3, T-Bet, Gata-3, Helios, IFN-γ, IL-4, IL-17A, IL-2, IL-10, OX40, Nrp1, GITR, pS6, p4EBP (eBioscience), ROR-γt, p_{T308}AKT (BD biosciences), p_{S473}AKT (Cell signaling) were used. Cell suspensions were incubated for 10 min with CD16/CD32 then stained for surface markers and viability dye for 20 min on PBS/0.5%FCS. Foxp3, Helios, T-Bet, Gata-3, ROR-γt and CTLA4 staining was performed overnight using the BD Cytofix/Cytoperm™ kit. For cytokine detection, cell suspensions were pre-incubated with 50 ng/mL PMA, 500 ng/mL ionomycin and 10 μg/mL brefeldin A for 4h in complete medium. Following CD16/32 blocking with specific mAbs, the cells were surface stained for the indicated markers then permeabilized and stained intracellularly overnight with mAbs against IL-2, IL-4, IL-10 IFN-γ, or IL-17 using the BD Cytofix/Cytoperm™ kit. For p_{S473}AKT, p_{T308}AKT, pS6 and p4EBP staining, spleen cells were stimulated for 30 min with soluble anti-CD3 mAb (1μg/mL), then fixed with PBS/2% paraformaldehyde for 20min, permeabilized in 90% methanol for 30 min on ice and stained for CD4, p_{S473}AKT and p_{T308}AKT or CD4, pS6 and p4EBP in PBS. For *ex-vivo* T_{reg} cell stimulation, isolated T_{reg} cells were cultured for 2 days with plate-bound anti-CD3 (1μg/mL) and IL-2 (100U/mL) in presence or absence of 2DG (Sigma; 2mg/mL) and PMA/ionomycin/BrefeldinA the last 4 hours before staining for IFN-γ and IL-4. All flow cytometry acquisitions were performed on a BD Fortessa cytometer using DIVA software (BD Biosystems) and analyzed using FlowJo Version 10 (Tree Star). All mouse and human antibodies used are listed in Supplementary Table 2 and 3, respectively.

Suppression assays

For mouse studies, $CD4^+YFP^-$ T_{eff} cells from $Foxp3^{EGFPcre}R26^{YFP}$ mice were isolated by cell sorting on FACSAria (Becton Dickinson), labeled with CellTrace™ Violet Cell Proliferation dye (Life Technologies) according to the manufacturer's instructions and used as responder cells. T_{reg} ($CD4^+YFP^+$) cells were similarly isolated by cell sorting and used as suppressor cells. Responder cells were cultured in triplicates at a fixed number of 10^5 cells/well in 96-well round-bottom plates and stimulated for 3 days with 1 μg/mL of soluble anti-CD3 mAb in the presence of 4×10^5 feeder spleen cells from $Rag1^{-/-}$ mice. In some experiments, T_{eff} and T_{reg} cells were pretreated for 1h with Rapamycin (Sigma; 1μM) or vehicle (DMSO), or 2DG (40mg/mL) or vehicle (PBS) overnight before being extensively washed and used as suppressor cells. For human studies, $CD4^+CD127^{hi}CD25^{lo}$ T cells from control subjects were by cell sorter, labeled with CellTrace™ Violet Cell Proliferation dye (Life technologies) according to the manufacturer's instructions and used as responder cells.

T_{reg} ($CD4^+CD127^{lo}CD25^{hi}$) cells were isolated on FACSAria from control or IPEX subjects and used as suppressor cells. Responder cells were cultured in triplicates at a fixed number of 5×10^4 cells per well and stimulated for 3 days with T cell activation and expansion beads (Miltenyi) in 96-well, round-bottom plates.

Adoptive transfer induced Colitis

Naïve (CD45.1 $CD4^+CD45RB^{high}GFP^-$) and T_{reg} ($CD4^+YFP^+$) cells are respectively isolated from the spleen of CD45.1 *Foxp3*^{EGFP} and CD45.2 *Foxp3*^{YFPCre} or *Foxp3*^{YFPCre}*Rictor*$^{\Delta/\Delta}$ mice. Colitis was induced in *Rag1*$^{-/-}$ males by i.p. injection of 5.10^5 CD45.1 naïve ± 5.10^4 T_{reg} cells. Mice were weighed and monitored for signs of disease twice weekly. Large intestines were dissected from the mice and the fecal contents were flushed out using PBS containing 2% FCS. The intestines were cut into 1cm pieces and treated with PBS containing 2% FCS, 1.5 mM dithiothreitol, and 10mM EDTA at 37 °C for 30 min with constant stirring to remove mucous and epithelial cells. The tissues were then minced and the cells were dissociated in RPMI containing collagenase (2 mg/mL collagenase II; Worthington), DNase I (100 μg/mL; Sigma), 5mM $MgCl_2$, 5mM $CaCl_2$, 5mM HEPES, and 10% FBS with constant stirring at 37 °C for 45 min. Leukocytes were collected at the interface of a 40%/70% Percoll gradient (GE Healthcare). The cells were washed with PBS containing 2% FCS and used for experiments.

Immunoblotting

Cell extracts were prepared by using RIPA buffer (50 mM Tris-HCl pH 7.4, 150 mM NaCl, 1 mM EDTA, 1% Triton X-100) supplemented with a complete protease inhibitor cocktail (Roche), a Phos STOP phosphatase inhibitor cocktail (Roche). The lysates were mixed with 4x loading buffer (Biorad) and denatured by heating for 5 minutes in 100°C. Samples were subjected to SDS-PAGE. The resolved proteins were then electrically transferred to a PVDF membrane (Millipore). Immunoblotting was probed with indicated antibodies followed by anti-rabbit IgG, HRP-linked antibody. The protein bands were visualized by using a SuperSignal West Pico chemiluminescence ECL kit (Pierce). Signal intensities of immunoblot bands were quantified by Image J software. For p_{Y319}-ZAP70 and ZAP70 immunoblotting, cell-sorted T_{reg} cells were stimulated with plate-bound anti-CD3 (145–2C11, 1 μg/mL) for 0, 2, 5 or 10 min prior protein extraction. A list of all antibodies used for immunoblotting is reported in Supplementary Table 4.

Metabolic profiling

Mouse splenocyte suspensions were enriched for $CD4^+$ T cells by positive selection with magnetic beads (Miltenyi). T_{reg} cells were cell sorted based on GFP expression and stimulated with plate-bound anti-CD3 (145–2C11, 1 μg/mL) and 100U recombinant mouse IL-2 (Peprotech) overnight. Sorted human T_{reg} ($CD4^+CD127^{lo}CD25^{hi}$) cells were isolated from blood after PBMCs enrichment by Ficoll-Paque (Sigma-Aldrich) density gradient centrifugation and treated with the competitive dual mTOR inhibitor KU 0063794 (Tocris) at 8 μg/mL or with vehicle (DMSO) in presence of T cell activation and expansion beads (Miltenyi) and 100U/mL of recombinant human IL-2 (Peprotech). Cells were washed and seeded in Seahorse 8 wells plate at 10^5 cells per well. ECAR and OCR were measured for both mouse and human T_{reg} cells using an XFp Extracellular Flux Analyzer respectively

under glycolysis, mitochondrial stress and mitochondrial fuel test conditions (Seahorse Bioscience-Agilent). For glycolysis stress test, assay buffer was made of non-buffered DMEM medium supplemented with 2 mM glutamine andD-glucose, Oligomycin and 2-DG were sequentially injected at a final concentration of 10mM, 1μM and 50mM, respectively. For Mitochondrial stress test, assay buffer was made of non-buffered DMEM medium supplemented with 2.5 mM D-glucose, 2 mM glutamine and 1 mM sodium pyruvate and Oligomycin, Carbonyl cyanide 4-(trifluoromethoxy)phenylhydrazone (FCCP) and Rotenone/ Antimycin A were sequentially injected at a final concentration of 1μM, 1μM and 500nM, respectively. For Mitochondrial fuel test, assay buffer was made of non-buffered DMEM medium supplemented with 2.5 mM D-glucose, 2 mM glutamine and 1 mM sodium pyruvate and UK5099, Etomoxir and Bis-2-(5-phenylacetamido-1,3,4-thiadiazol-2-yl)ethyl sulfide (BPTES) were sequentially injected at a final concentration of 2μM, 4μM and 3μM, respectively. Baseline ECAR (for glycolysis stress test) and OCR (for mitochondrial stress and mitochondrial fuel tests) values were averaged between technical replicates for these first three successive time intervals. For lactate production by ELISA, 10^5 purified mouse naïve T_{eff} cells ($CD4^+CD62L^{hi}CD44^{lo}$) from *Foxp3*^{EGFP} mice or T_{reg} cells from *Foxp3*^{EGFP}, *Foxp3*$^{\Delta EGFPiCre}$ and *Foxp3*$^{\Delta EGFPiCre}$*Rictor*$^{\Delta/\Delta}$ mice were seeded in flat bottom 96 well plate in complete RPMI medium in absence or presence of plate-bound anti-CD3 (1μg/mL) and 100U/mL of recombinant IL-2. Supernatants were collected after 48h and extracellular lactate production was measured using L-Lactate Assay Kit (Abcam). For metabolomics profiling, 2.5×10^6 purified T_{reg} cells from *Foxp3*^{EGFP}, *Foxp3*$^{\Delta EGFPiCre}$ and *Foxp3*$^{\Delta EGFPiCre}$*Rictor*$^{\Delta/\Delta}$ mice were seeded in flat bottom 48 well plate in complete RPMI medium in presence of plate-bound anti-CD3 (1μg/mL) and 100U/mL of recombinant IL-2. Supernatants and cell pellets were collected after 48h and analyzed for metabolomics studies (Metabolom ®, Morrisville, North Carolina, USA).

Transcriptome profiling

Splenic T_{reg} ($CD4^+$RFP+ or $CD4^+YFP^+$) cells were double-sorted from 4 weeks old female *Foxp3*$^{\Delta EGFPiCre/RFP}$*R26*^{YFP} and *Foxp3*$^{\Delta EGFPiCre/+}$*Rictor*$^{\Delta/\Delta}$*R26*^{YFP} mice. (n=4 per group). Cells were collected directly into TRIzol (Invitrogen). Total RNA was extracted and converted into double-stranded DNA (dsDNA), using SMART-Seq v4 Ultra Low Input RNA kit (Clontech). dsDNA was then fragmented to 200- to 300-bp-sized fragments, using M220 Focused-ultrasonicator (Covaris), and these were used for the construction of libraries for Illumina sequencing, using the KAPA Hyper Prep Kit (Kapa Biosystems). Libraries were then quantified using Qubit dsDNA HS (high-sensitivity) Assay Kit on Agilent High Sensitivity DNA Bioanalyzer. RNA sequencing data was demultiplexed by using perfect matches to indices and was quality-inspected using FastQC. The sequencing data was aligned to the mm10 build (Gencode annotation) of the mouse genome using STAR62, and counts were quantified using HTSeq63. Raw counts were filtered for non-mitochondrial protein-coding genes with at least three counts in one sample, and were normalized using the DESeq2 package in R64. Pairwise comparisons of differential gene expression were computed using DESeq2.

Histology

Large intestine, lung, Liver and ear sections were stained with hematoxylin and eosin. Histopathological scoring of tissue was done by a blinded observer, and the final scores reflected averages of scores from 5 different ×200 fields per tissue per mouse. Large intestinal sections were scored as follows [53]: 0, no inflammation; 1, mild, scattered infiltrates; 2, moderate infiltrates without loss of epithelium integrity; 3, moderate and diffuse or severe inflammation; 4, Severe inflammation associated with loss of the epithelial barrier integrity. Lung inflammation was scored separately for cellular infiltration around blood vessels and airways, as follows: 0, no infiltrates; 1, few inflammatory cells; 2, a ring of inflammatory cells 1 cell layer deep; 3, a ring of inflammatory cells 2–4 cells deep; 4, a ring of inflammatory cells >4 cells deep. A composite score was determined by adding the inflammatory scores for both vessels and airways. Liver inflammation was scored at portal areas, as follows: 0, no inflammatory cells; 1, mild, scattered infiltrates; 2, moderate infiltrates occupying less than 50% of the portal areas; 3, extensive infiltrates in the portal areas; 4, severe, with infiltrates completely packing the portal area and spilling over into the parenchyma. Ear inflammation was scored as followed: 0, no inflammation, no infiltration; Mild inflammation associated with few cells infiltration; 2, moderately severe inflammation associated with mild infiltration; 3, severe inflammation associated with large infiltration of cells and mild skin dryness; 4, very severe inflammation associated with skin dryness and cartilage erosion.

Methylation analysis

The methylation status of *Foxp3* T_{reg}-specific demethylation region (TSDR or CNS2) in splenic T_{reg} cells of 25 d old male mice was assessed by bisulfite sequence analysis, as described [54]. The TSDR of converted DNA was amplified by methylation-specific primer sequences: *Foxp3 CNS2* Forward 5’-TATTTTTTTGGGTTTTGGGATATTA-3’ (forward) and *Foxp3 CNS2* Reverse 5’-AACCAACCAACTTCCTACACTATCTAT-3’. The PCR product was subcloned and sequenced [54]. Blast analyses were done by comparing the resulting sequences with converted *Foxp3* gene sequences.

Confocal microscopy

Confocal microscopic analysis of Foxo1 nuclear and cytoplasmic distribution was carried out as described [28]. T_{reg} cells were purified and incubated on pre-coated coverslip (poly-L-lysin 50 μg/mL, ± anti-CD3 0.1 μg/mL) at 37°C for 30 min in RPMI/10%FCS. After fixation with PBS/4% paraformaldehyde, cells were permeabilized with PBS/0.1% saponin and blocked on PBS/4% bovine serum albumin (BSA). Cells were incubated with 1:100 diluted rabbit anti-Foxo1 (C29H4, Cell Signaling) followed by 1:500 diluted Alexa fluor 555-anti rabbit secondary antibody (Life technologies) in PBS/1%BSA. Slides were mounted with gold anti-fade reagent with DAPI (Invitrogen). Images were acquired with a Zeiss LSM700 confocal microscopy and ZEN imaging software. Five to 10 fields were selected randomly and total cells in the field were analyzed for percentage of Foxo1 nuclear localization using ImageJ software. Percentage of nuclear Foxo1 localization was obtained by the formula: 100 X corrected nuclear fluorescence/corrected total cell fluorescence and

corrected fluorescence was obtained by the formula: Integrated Density – (Area of selected cell or nucleus X Mean fluorescence of background).

Chromatin Immunoprecipitation

ΔT_{reg} cells were isolated from spleen of *Foxp3*$^{\Delta EGFPiCre}$ and *Foxp3*$^{\Delta EGFPiCre}$*Rictor*$^{\Delta/\Delta}$ mice. Cells were first cross-linked with 10% paraformaldehyde (PFA) for 8 minutes at room temperature (RT). Chromatin was centrifuged and the pellet was resuspended in lysis buffer I for 20 minutes at RT. The chromatin was pelleted again at 8000 rpm for 5 min at 4°C. The chromatin was then resuspended in 75 μl lysis buffer II containing 4% SDS. The chromatin was incubated for 5 min at RT to ensure the disruption of the nucleus and the release of the chromatin. The supernatant was then diluted to 1% SDS content using lysis buffer II without any SDS. Afterwards, the chromatin was sonicated using the bioruptor (Diagenode, Denville, NJ, USA) toward a proper size of 200–400 bp per DNA fragment for further immunoprecipitation. For the chromatin immunoprecipitation (ChIP) 3 antibodies were used to pull down the DNA fragments. Blimp1 (clone 3H2-E8, Invitrogen, USA), Foxo1 (clone 3B6, Invitrogen, USA) and mock IgG1 isotype control (Invitrogen, USA). Quantitative RT-PCR with the precipitated chromatin was performed to calculate the percentage of input and a fold change Blimp1/Isotype control or Foxo1/Isotype control was performed for each sample. All amplifications were performed in triplicate with SYBR Green PCR Master Mix (Qiagen) and specific primers for the different locations (5'-CTTGAGGAAAAGCCAGCATC-3' Forward and 5'-TTTGCGTGTTCACCTGTGTT-3' Reverse primers for il10 CNS–9, 5'-AGGCGAGATCTGAAGTGCAT-3' Forward and 5'-CCTGCCGGTTGTAATCAACT-3' Reverse primers for *Tbx21* Promoter and 5'-TACTTCCTGCTCAGACCTGC-3' Forward and 5'-TTCCCATCTCCTTCCTGTGG-3' Reverse primers for *Ifng* Promoter). Control ChIP was performed with a respective isotype control antibody to ensure specificity. After normalization of the data according to the isotype control, the specific pulldown (percentage of input chromatin) was calculated.

Statistical analysis

Data were analyzed by paired and unpaired two-tailed Student's *t*-test, one- and two-way ANOVA with post-test analyses and log-rank test, as indicated. Differences in mean values were considered significant at a $P < 0.05$.

Data Availability

Data presented in the manuscript, including de-identified patient results, will be made available to investigators following request to the corresponding author. Any data and materials to be shared will be released via a Material Transfer Agreement. RNAseq datasets have been deposited in the GEO with the accession code GSE129472.

Supplementary Material

Refer to Web version on PubMed Central for supplementary material.

Acknowledgements

This work was supported by a National Institutes of Health grants 2R01 AI065617 (to T.A.C.) and RO1 AI102888-01A1 (to M.L).

References

1. Josefowicz SZ, Lu LF & Rudensky AY Regulatory T cells: mechanisms of differentiation and function. Annu Rev Immunol 30, 531–564 (2012). [PubMed: 22224781]
2. Nutsch KM & Hsieh CS T cell tolerance and immunity to commensal bacteria. Curr Opin Immunol 24, 385–391 (2012). [PubMed: 22613090]
3. Lin W et al. Regulatory T cell development in the absence of functional Foxp3. Nat Immunol 8, 359–368 (2007). [PubMed: 17273171]
4. Gavin MA et al. Foxp3-dependent programme of regulatory T-cell differentiation. Nature 445, 771–775 (2007). [PubMed: 17220874]
5. Ohkura N et al. T cell receptor stimulation-induced epigenetic changes and Foxp3 expression are independent and complementary events required for Treg cell development. Immunity 37, 785–799 (2012). [PubMed: 23123060]
6. Kaech SM & Cui W Transcriptional control of effector and memory CD8+ T cell differentiation. Nat Rev Immunol 12, 749–761 (2012). [PubMed: 23080391]
7. Rudensky AY Regulatory T cells and Foxp3. Immunol Rev 241, 260–268 (2011). [PubMed: 21488902]
8. Buck MD, Sowell RT, Kaech SM & Pearce EL Metabolic Instruction of Immunity. Cell 169, 570–586 (2017). [PubMed: 28475890]
9. Beier UH et al. Essential role of mitochondrial energy metabolism in Foxp3(+) T-regulatory cell function and allograft survival. FASEB J 29, 2315–2326 (2015). [PubMed: 25681462]
10. Gerriets VA et al. Metabolic programming and PDHK1 control CD4+ T cell subsets and inflammation. J Clin Invest 125, 194–207 (2015). [PubMed: 25437876]
11. Michalek RD et al. Cutting edge: distinct glycolytic and lipid oxidative metabolic programs are essential for effector and regulatory CD4+ T cell subsets. J Immunol 186, 3299–3303 (2011). [PubMed: 21317389]
12. Shi LZ et al. HIF1alpha-dependent glycolytic pathway orchestrates a metabolic checkpoint for the differentiation of TH17 and Treg cells. J Exp Med 208, 1367–1376 (2011). [PubMed: 21708926]
13. Angelin A et al. Foxp3 Reprograms T Cell Metabolism to Function in Low-Glucose, High-Lactate Environments. Cell Metab 25, 1282–1293 e1287 (2017). [PubMed: 28416194]
14. Gerriets VA et al. Foxp3 and Toll-like receptor signaling balance Treg cell anabolic metabolism for suppression. Nat Immunol 17, 1459–1466 (2016). [PubMed: 27695003]
15. Pollizzi KN & Powell JD Regulation of T cells by mTOR: the known knowns and the known unknowns. Trends Immunol 36, 13–20 (2015). [PubMed: 25522665]
16. Chapman NM & Chi H mTOR Links Environmental Signals to T Cell Fate Decisions. Frontiers in immunology 5, 686 (2014). [PubMed: 25653651]
17. Valmori D et al. Rapamycin-mediated enrichment of T cells with regulatory activity in stimulated CD4+ T cell cultures is not due to the selective expansion of naturally occurring regulatory T cells but to the induction of regulatory functions in conventional CD4+ T cells. J Immunol 177, 944–949 (2006). [PubMed: 16818749]
18. Liu C, Chapman NM, Karmaus PW, Zeng H & Chi H mTOR and metabolic regulation of conventional and regulatory T cells. J Leukoc Biol (2015).
19. Delgoffe GM et al. The mTOR kinase differentially regulates effector and regulatory T cell lineage commitment. Immunity 30, 832–844 (2009). [PubMed: 19538929]
20. Zeng H et al. mTORC1 couples immune signals and metabolic programming to establish T(reg)-cell function. Nature 499, 485–490 (2013). [PubMed: 23812589]
21. Sarbassov DD, Guertin DA, Ali SM & Sabatini DM Phosphorylation and regulation of Akt/PKB by the rictor-mTOR complex. Science 307, 1098–1101 (2005). [PubMed: 15718470]

22. Manning BD & Toker A AKT/PKB Signaling: Navigating the Network. Cell 169, 381–405 (2017). [PubMed: 28431241]
23. Patterson SJ et al. Cutting edge: PHLPP regulates the development, function, and molecular signaling pathways of regulatory T cells. J Immunol 186, 5533–5537 (2011). [PubMed: 21498666]
24. Shrestha S et al. Treg cells require the phosphatase PTEN to restrain TH1 and TFH cell responses. Nat Immunol 16, 178–187 (2015). [PubMed: 25559258]
25. Williams BL et al. Phosphorylation of Tyr319 in ZAP-70 is required for T-cell antigen receptor-dependent phospholipase C-gamma1 and Ras activation. EMBO J 18, 1832–1844 (1999). [PubMed: 10202147]
26. Lin W et al. Allergic dysregulation and hyperimmunoglobulinemia E in Foxp3 mutant mice. J Allergy Clin Immunol 116, 1106–1115 (2005). [PubMed: 16275384]
27. Leach MW, Bean AG, Mauze S, Coffman RL & Powrie F Inflammatory bowel disease in C.B-17 scid mice reconstituted with the CD45RBhigh subset of CD4+ T cells. Am J Pathol 148, 1503–1515 (1996). [PubMed: 8623920]
28. Charbonnier LM, Wang S, Georgiev P, Sefik E & Chatila TA Control of peripheral tolerance by regulatory T cell-intrinsic Notch signaling. Nat Immunol 16, 1162–1173 (2015). [PubMed: 26437242]
29. Wan YY & Flavell RA Identifying Foxp3-expressing suppressor T cells with a bicistronic reporter. Proc Natl Acad Sci U S A 102, 5126–5131 (2005). [PubMed: 15795373]
30. Gan X et al. PRR5L degradation promotes mTORC2-mediated PKC-delta phosphorylation and cell migration downstream of Galpha12. Nature cell biology 14, 686–696 (2012). [PubMed: 22609986]
31. Neumann C et al. Role of Blimp-1 in programing Th effector cells into IL-10 producers. J Exp Med 211, 1807–1819 (2014). [PubMed: 25073792]
32. Plas DR & Thompson CB Akt activation promotes degradation of tuberin and FOXO3a via the proteasome. J Biol Chem 278, 12361–12366 (2003). [PubMed: 12517744]
33. Ouyang W et al. Novel Foxo1-dependent transcriptional programs control T(reg) cell function. Nature 491, 554–559 (2012). [PubMed: 23135404]
34. Kerdiles YM et al. Foxo transcription factors control regulatory T cell development and function. Immunity 33, 890–904 (2010). [PubMed: 21167754]
35. Hagiwara A et al. Hepatic mTORC2 Activates Glycolysis and Lipogenesis through Akt, Glucokinase, and SREBP1c. Cell Metabolism 15, 725–738 (2012). [PubMed: 22521878]
36. Wilhelm K et al. FOXO1 couples metabolic activity and growth state in the vascular endothelium. Nature 529, 216–220 (2016). [PubMed: 26735015]
37. Pearce EL, Poffenberger MC, Chang CH & Jones RG Fueling immunity: insights into metabolism and lymphocyte function. Science 342, 1242454 (2013). [PubMed: 24115444]
38. Huynh A et al. Control of PI(3) kinase in Treg cells maintains homeostasis and lineage stability. Nat Immunol 16, 188–196 (2015). [PubMed: 25559257]
39. Wang R et al. The transcription factor Myc controls metabolic reprogramming upon T lymphocyte activation. Immunity 35, 871–882 (2011). [PubMed: 22195744]
40. Longo N, Frigeni M & Pasquali M Carnitine transport and fatty acid oxidation. Biochim Biophys Acta 1863, 2422–2435 (2016). [PubMed: 26828774]
41. De Bock K et al. Role of PFKFB3-driven glycolysis in vessel sprouting. Cell 154, 651–663 (2013). [PubMed: 23911327]
42. Chatila TA et al. JM2, encoding a fork head-related protein, is mutated in X-linked autoimmunity-allergic disregulation syndrome. J Clin Invest 106, R75–81 (2000). [PubMed: 11120765]
43. Bacchetta R et al. Defective regulatory and effector T cell functions in patients with FOXP3 mutations. J Clin Invest 116, 1713–1722 (2006). [PubMed: 16741580]
44. Gavin MA et al. Single-cell analysis of normal and FOXP3-mutant human T cells: FOXP3 expression without regulatory T cell development. Proc Natl Acad Sci U S A 103, 6659–6664 (2006). [PubMed: 16617117]
45. Bacchetta R, Barzaghi F & Roncarolo MG From IPEX syndrome to FOXP3 mutation: a lesson on immune dysregulation. Annals of the New York Academy of Sciences (2016).

46. Liu W et al. CD127 expression inversely correlates with FoxP3 and suppressive function of human CD4+ T reg cells. J Exp Med 203, 1701–1711 (2006). [PubMed: 16818678]
47. Seddiki N et al. Expression of interleukin (IL)-2 and IL-7 receptors discriminates between human regulatory and activated T cells. J Exp Med 203, 1693–1700 (2006). [PubMed: 16818676]
48. Zhang L et al. Mammalian Target of Rapamycin Complex 2 Controls CD8 T Cell Memory Differentiation in a Foxo1-Dependent Manner. Cell reports 14, 1206–1217 (2016). [PubMed: 26804903]
49. Hayatsu N et al. Analyses of a Mutant Foxp3 Allele Reveal BATF as a Critical Transcription Factor in the Differentiation and Accumulation of Tissue Regulatory T Cells. Immunity (2017).
50. Bin Dhuban K et al. Suppression by human FOXP3+ regulatory T cells requires FOXP3-TIP60 interactions. Sci Immunol 2 (2017).
51. Bennett CL et al. A rare polyadenylation signal mutation of the FOXP3 gene (AAUAAA-->AAUGAA) leads to the IPEX syndrome. Immunogenetics 53, 435–439 (2001). [PubMed: 11685453]
52. Raymond CS & Soriano P High-efficiency FLP and PhiC31 site-specific recombination in mammalian cells. PLoS One 2, e162 (2007). [PubMed: 17225864]
53. Rivas MN et al. MyD88 is critically involved in immune tolerance breakdown at environmental interfaces of Foxp3-deficient mice. J Clin Invest 122, 1933–1947 (2012). [PubMed: 22466646]
54. Schmitt EG et al. IL-10 produced by induced regulatory T cells (iTregs) controls colitis and pathogenic ex-iTregs during immunotherapy. J Immunol 189, 5638–5648 (2012). [PubMed: 23125413]

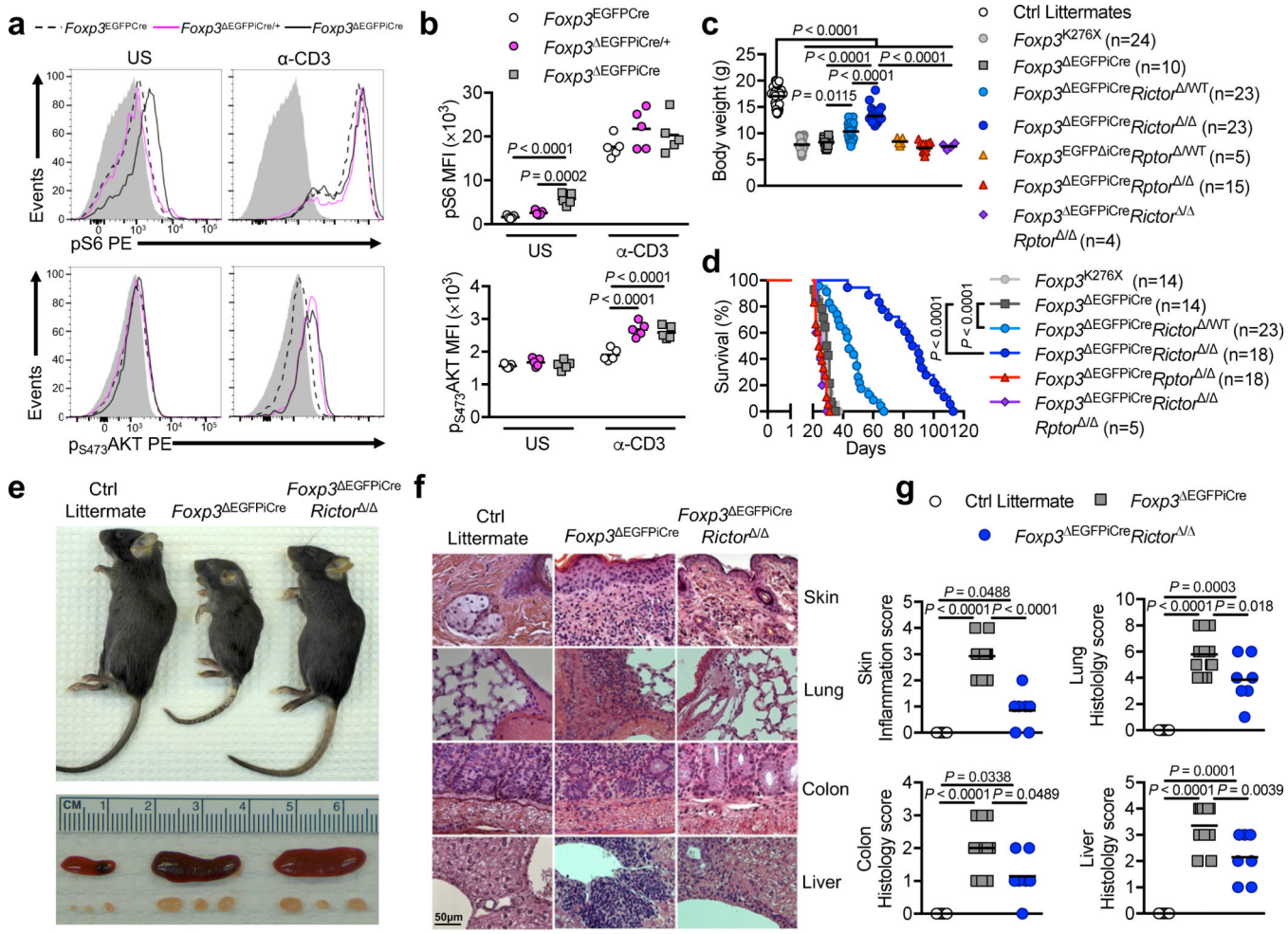

Figure 1. Inactivation of mTORC2 but not mTORC1 in ΔT_{reg} cells mitigates Foxp3 deficiency.

(**a,b**) Representative flow cytometric analysis (**a**) and mean fluorescence intensity (MFI) (**b**) of phosphorylated S6 (pS6) and phosphorylated AKT at Ser473 residu ($pS_{473}AKT$) expression of unstimulated (US) or anti-CD3 stimulated (α-CD3) T_{reg} cells from *Foxp3*^{EGFPCre}, *Foxp3*$^{\Delta EGFPiCre/+}$ and *Foxp3*$^{\Delta EGFPiCre}$ mice (n=5 per group). Results represent 1 of 3 independent experiments. (**c,d**) Body weight at 25–28 days of age (**c**) and survival (**d**) of *Foxp3*^{K276X}, *Foxp3*$^{\Delta EGFPiCre}$, *Foxp3*$^{\Delta EGFPiCre}$*Rictor*$^{\Delta/WT}$, *Foxp3*$^{\Delta EGFPiCre}$*Rictor*$^{\Delta/\Delta}$, *Foxp3*$^{\Delta EGFPiCre}$*Rptor*$^{\Delta/WT}$, *Foxp3*$^{\Delta EGFPiCre}$*Rptor*$^{\Delta/\Delta}$, *Foxp3*$^{\Delta EGFPiCre}$*Rictor*$^{\Delta/\Delta}$*Rptor*$^{\Delta/\Delta}$ mice and control littermates. Results represent a pool of 5 independent experiments. (**e**) Gross appearance of *Foxp3*$^{\Delta EGFPiCre}$, *Foxp3*$^{\Delta EGFPiCre}$*Rictor*$^{\Delta/\Delta}$ and control littermate and their respective spleens and peripheral lymph nodes. (**f,g**) Representative microscopic pictures of H&E staining (original magnification ×200) (**f**) and histological scores (**g**) of skin, lung, colon and liver of *Foxp3*$^{\Delta EGFPiCre}$ (n=14), *Foxp3*$^{\Delta EGFPiCre}$*Rictor*$^{\Delta/\Delta}$ (n=7) and control littermates (n=5). Results represent a pool of 3 independent experiments. Statistical significance was determined by a one-way ANOVA with Tukey's multiple comparisons (**c**, **g**), two-way ANOVA with Sidak's multiple comparisons (**b**) and log rank test (**d**) (*P* values as indicated).

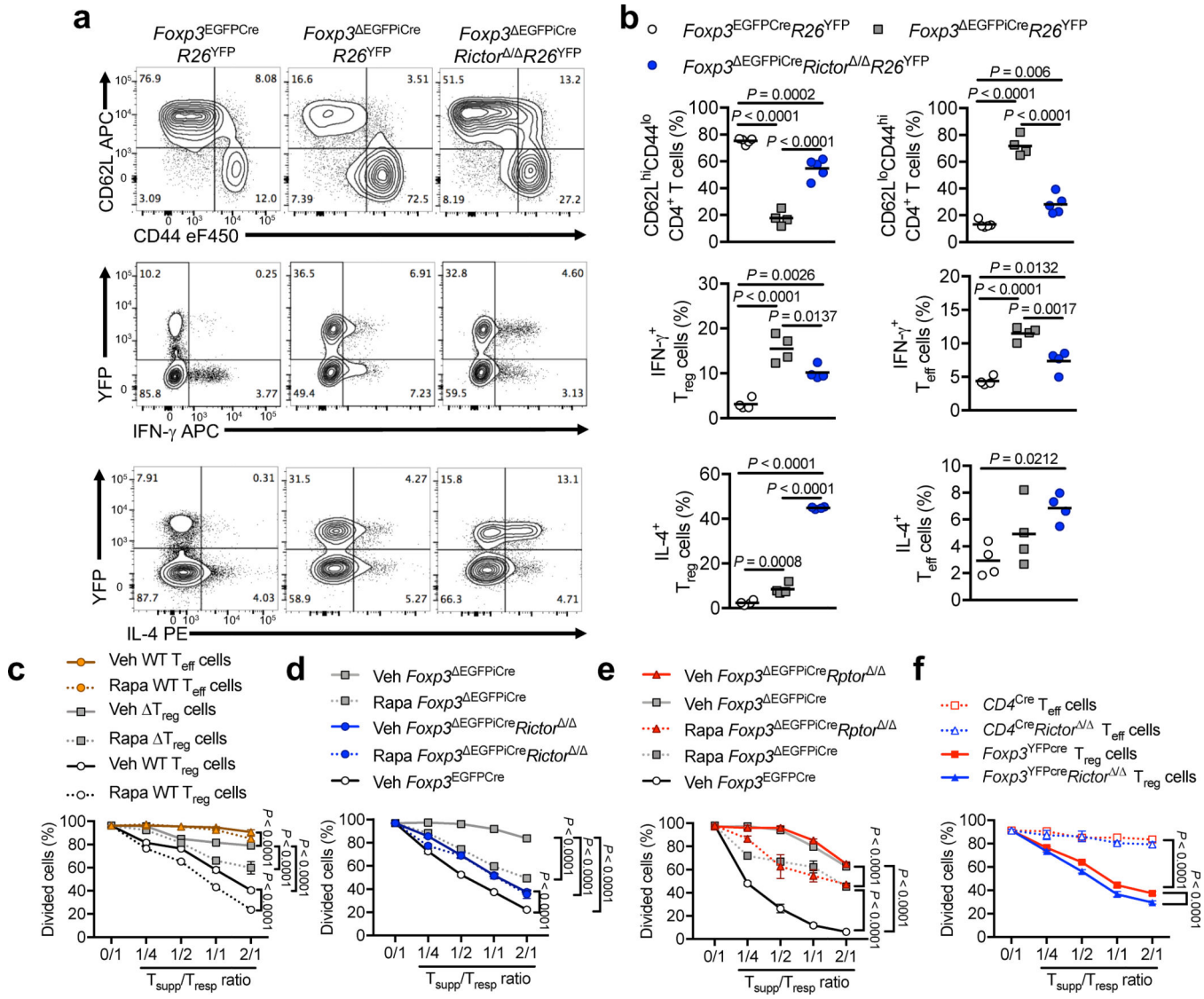

Figure 2. mTORC2 blockade endows ΔT_{reg} cells with regulatory function.

(**a,b**) Representative flow cytometric analysis (**a**) and frequencies (scatter plots with mean) (**b**) of $CD62L^{hi}CD44^{lo}$ and $CD62L^{lo}CD44^{hi}$ $CD4^+$ T cells or IFN-γ and IL-4 expression by $CD4^+$ T_{reg} (YFP^+) and T_{eff} (YFP^-) cells from spleen of *Foxp3*^{EGFPCre}R26^{YFP} (n=5 for $CD62L^{hi}CD44^{lo}$ and $CD62L^{lo}CD44^{hi}$ $CD4^+$ T cells, n=4 for IFN-γ and IL-4 expression), *Foxp3*$^{\Delta EGFPiCre}$R26^{YFP} (n=4) and *Foxp3*$^{\Delta EGFPiCre}$*Rictor*$^{\Delta/\Delta}$R26^{YFP} mice (n=5 for $CD62L^{hi}CD44^{lo}$ and $CD62L^{lo}CD44^{hi}$ $CD4^+$ T cells, n=4 for IFN-γ and IL-4 expression). Results represent 1 of 4 independent experiments (**c**) In vitro suppression of the proliferation of WT $CD4^+$ T_{eff} cells (denoted as T responder or T_{resp}) by *Foxp3*^{EGFPCre} T_{eff} cells pre-treated for 1h with DMSO (Veh WT T_{eff} cells) or 1μM Rapamycin (Rapa WT T_{eff} cells), *Foxp3*^{EGFPCre} T_{reg} cells pre-treated for 1h with DMSO (Veh WT T_{reg} cells) or 1μM Rapamycin (Rapa WT T_{reg} cells) or *Foxp3*$^{\Delta EGFPiCre}$ T_{reg} cells pre-treated for 1h with DMSO (Veh ΔT_{reg} cells) or 1μM Rapamycin (Rapa ΔT_{reg} cells) (denoted as T suppressor or T_{supp}) (n=3 per group). Results represent 1 of 3 independent experiments (**d, e**) In vitro

suppression of T_{resp} cells by *Foxp3*^{EGFPCre} T_{reg} cells (*Foxp3*^{EGFPCre}), *Foxp3*$^{\Delta EGFPiCre}$ T_{reg} cells pre-treated for 1h with DMSO (Veh *Foxp3*$^{\Delta EGFPiCre}$) or 1μM Rapamycin (Rapa *Foxp3*$^{\Delta EGFPiCre}$), *Foxp3*$^{\Delta EGFPiCre}$*Rictor*$^{\Delta/\Delta}$ T_{reg} cells pre-treated for 1h with DMSO (Veh *Foxp3*$^{\Delta EGFPiCre}$*Rictor*$^{\Delta/\Delta}$) or 1μM Rapamycin (Rapa *Foxp3*$^{\Delta EGFPiCre}$*Rictor*$^{\Delta/\Delta}$) (n=3 per group) (Results represent 1 of 3 independent experiments) (**d**), and *Foxp3*$^{\Delta EGFPiCre}$*Rptor*$^{\Delta/\Delta}$ T_{reg} cells pre-treated for 1h with DMSO (Veh *Foxp3*$^{\Delta EGFPiCre}$*Rptor*$^{\Delta/\Delta}$) or 1μM Rapamycin (Rapa *Foxp3*$^{\Delta EGFPiCre}$*Rptor*$^{\Delta/\Delta}$) (n=3 per group) (Results represent 1 of 3 independent experiments) (**e**). (**f**) In vitro suppression of T_{resp} cells by Rictor-sufficient or -deficient T_{eff} ($CD4^+CD25^-$ cells from *CD4*^{cre} and *CD4*^{cre}*Rictor*$^{\Delta/\Delta}$) and Foxp3-sufficient T_{reg} (*Foxp3*^{YFPcre} and *Foxp3*^{YFPcre}*Rictor*$^{\Delta/\Delta}$) cells (n=3 per group) (Results represent 1 of 2 independent experiments). Results are expressed as mean ± SEM in panels **c-f**. Statistical significance was determined by a one-way ANOVA (**b**) or two-way ANOVA with Tukey's multiple comparisons (**c-f**) (*P* values as indicated).

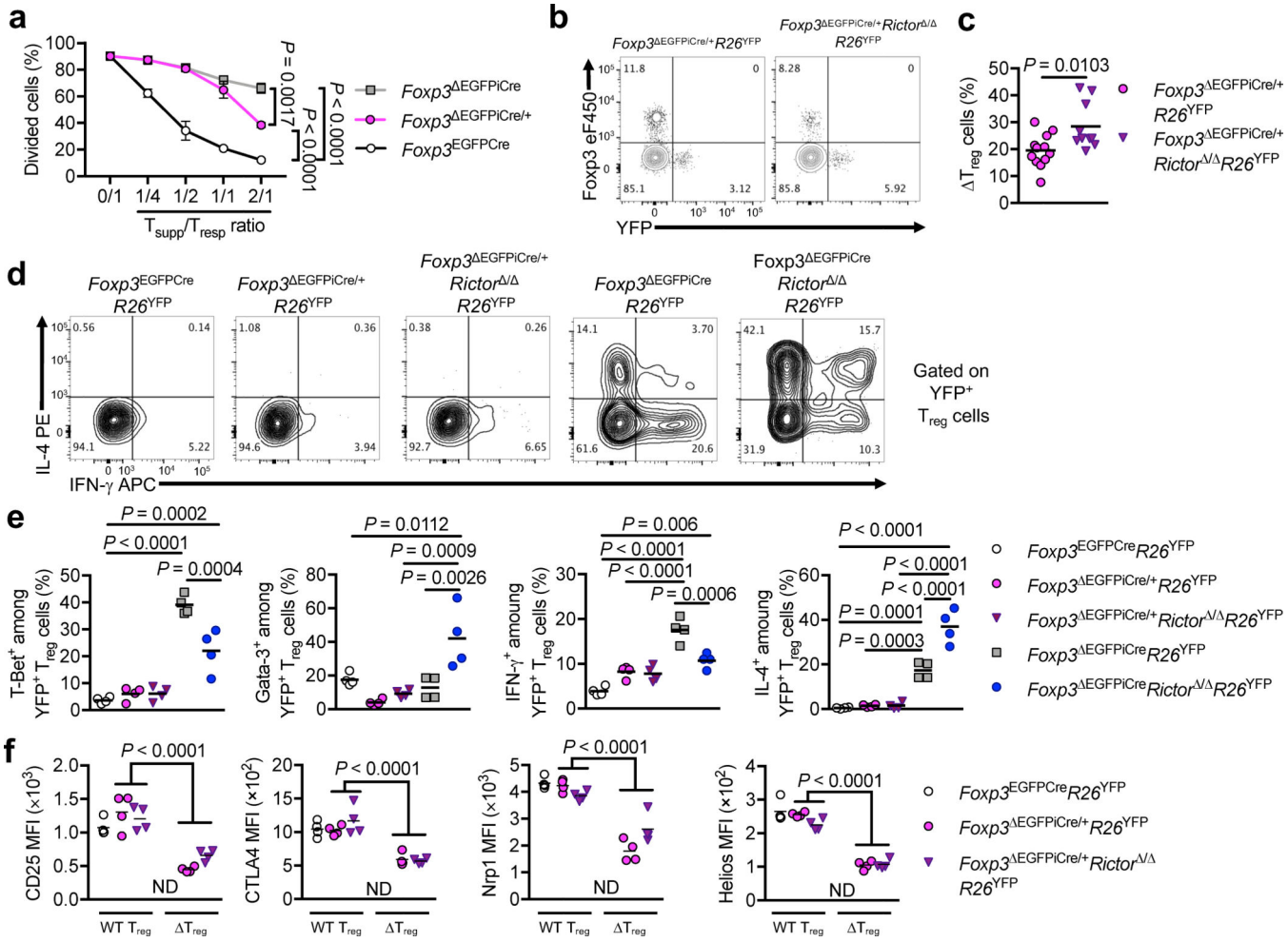

Figure 3: Cell intrinsic and extrinsic determinants of the T_{eff} cell-like phenotype of ΔT_{reg} cells.

(**a**) In vitro suppression of CD4$^+$ T_{eff} cell (T_{resp}) proliferation by Foxp3-sufficient T_{reg} cells from *Foxp3*^{EGFPcre} mice and ΔT_{reg} cells from *Foxp3*$^{\Delta EGFPiCre/+}$ and *Foxp3*$^{\Delta EGFPiCre}$ mice (T_{supp}) (n=3 per group). Results are expressed as mean ± SEM and represent 1 of 2 independent experiments. (**b**, **c**) Representative flow cytometric analysis of Foxp3 and YFP among CD4$^+$ T cells (**b**) and frequencies of ΔT_{reg} cells (**c**) among total T_{reg} cells from *Foxp3*$^{\Delta EGFPiCre/+}$*R26*^{YFP} (n=12) and *Foxp3*$^{\Delta EGFPiCre/+}$*Rictor*$^{\Delta/\Delta}$*R26*^{YFP} (n=10) mice. Results are expressed as scatter plot and mean and represent a pool of 3 independent experiments. (**d**, **e**) Representative flow cytometric analysis of IL-4 and IFN-γ among YFP$^+$ T_{reg} cells (**d**) and frequencies (Scatter plot and mean) of T-Bet$^+$, Gata-3$^+$, IFN-γ$^+$ and IL-4$^+$ YFP$^+$ T_{reg} cells (**e**) from *Foxp3*^{EGFPCre}*R26*^{YFP}, *Foxp3*$^{\Delta EGFPiCre/+}$*R26*^{YFP}, *Foxp3*$^{\Delta EGFPiCre/+}$*Rictor*$^{\Delta/\Delta}$*R26*^{YFP}, *Foxp3*$^{\Delta EGFPiCre}$*R26*^{YFP} and *Foxp3*$^{\Delta EGFPiCre}$*Rictor*$^{\Delta/\Delta}$*R26*^{YFP} mice (n=4 per group). Results represent 1 of 2 independent experiments. (**f**) CD25, CTLA4, Nrp1 and Helios MFI in WT T_{reg} and ΔT_{reg} cells from *Foxp3*^{EGFPCre}*R26*^{YFP}, *Foxp3*$^{\Delta EGFPiCre/+}$*R26*^{YFP}, *Foxp3*$^{\Delta EGFPiCre/+}$*Rictor*$^{\Delta/\Delta}$*R26*^{YFP} female mice (n=4 per group). ND, Not Determined. Results represent 1 of 2 independent experiments. Statistical significance was determined by unpaired t-test (**c**), one-way ANOVA (**e**) or two-way ANOVA (**a, f**) with Tukey's multiple comparisons (*P* values as indicated).

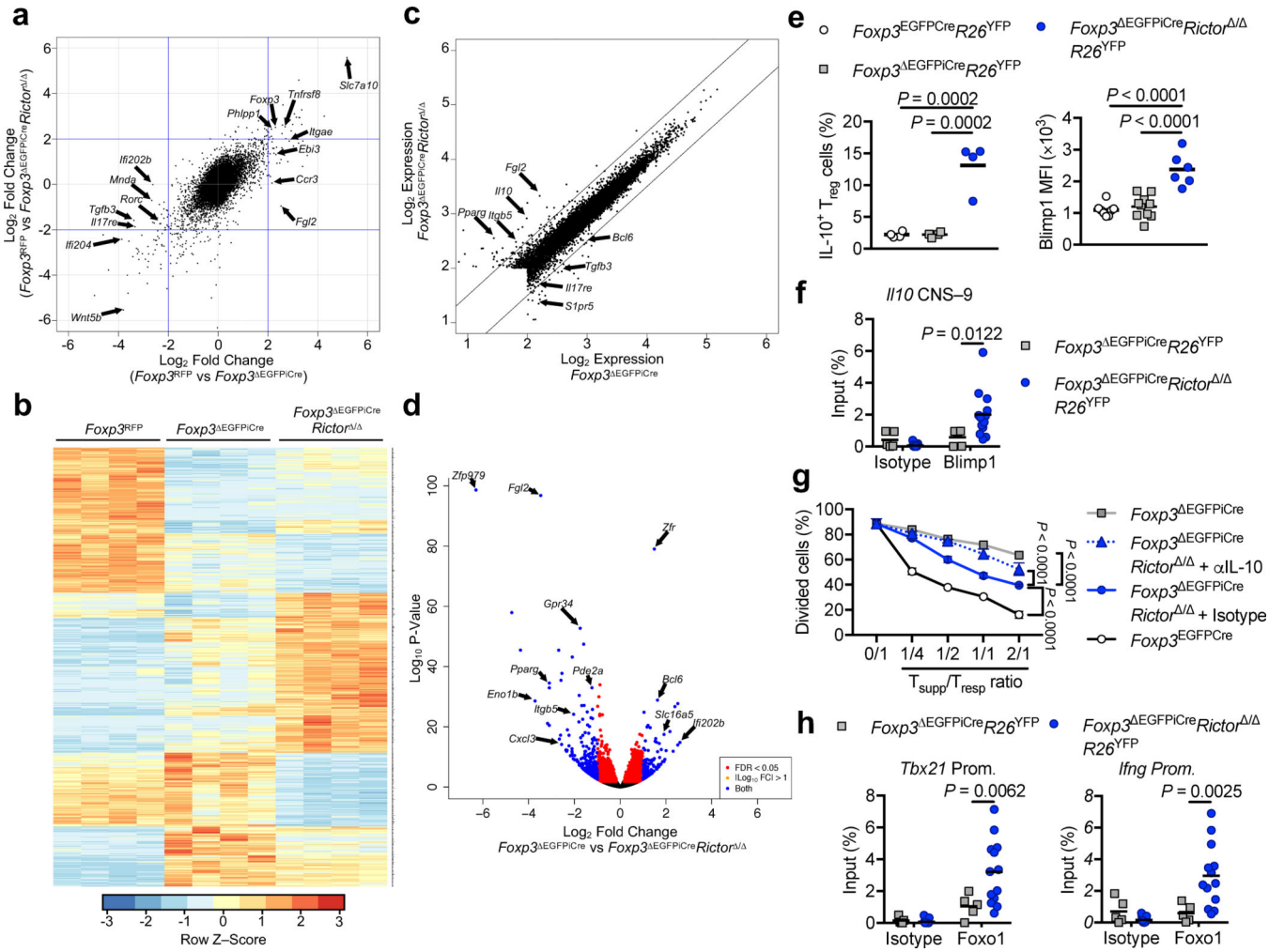

Figure 4. mTORC2-dependent and -independent gene expression profiles in ΔT_{reg} cells.

Gene expression profiles of Foxp3^{RFP} (WT), *Foxp3*$^{\Delta EGFPiCre}$ and *Foxp3*$^{\Delta EGFPiCre}$*Rictor*$^{\Delta/\Delta}$ T_{reg} cells (n=4 per group) isolated from spleen of Foxp3$^{RFP/\Delta EGFPiCre}$*R26*^{YFP} and Foxp3$^{\Delta EGFPiCre/+}$*Rictor*$^{\Delta/\Delta}$*R26*^{YFP} female mice. (**a**), Gene expression profiles represented as Fold change (*Foxp3*^{RFP} vs *Foxp3*$^{\Delta EGFPiCre}$) versus Fold change (*Foxp3*^{RFP} vs *Foxp3*$^{\Delta EGFPiCre}$*Rictor*$^{\Delta/\Delta}$). (**b**), Heatmap representation, (**c**), Log_2 expression and (**d**) volcano plot of differential gene expression in *Foxp3*$^{\Delta EGFPiCre}$ versus *Foxp3*$^{\Delta EGFPiCre}$*Rictor*$^{\Delta/\Delta}$ ΔT_{reg} cells. FDR, false discovery rate; log2FC, log2(fold change). (**e**), Flow cytometric analysis of IL-10 and Blimp1 expression in T_{reg} cells of *Foxp3*^{EGFPCre} (n=4 and n=8 respectively) and ΔT_{reg} cells of *Foxp3*$^{\Delta EGFPiCre}$ (n=4 and n=10 respectively) and *Foxp3*$^{\Delta EGFPiCre}$*Rictor*$^{\Delta/\Delta}$ (n=4 and n=6 respectively) mice. Results are expressed as scatter plot and mean and represent 1 of 3 independent experiments. (**f**), Chromatin immunoprecipitation (ChIP) assay for the binding of Blimp1 and control isotype to the *Il10* conserved non-coding sequence located 9kb in proximal of *il10* promoter (*il10 CNS–9*) in *Foxp3*$^{\Delta EGFPiCre}$ (n=5) and *Foxp3*$^{\Delta EGFPiCre}$*Rictor*$^{\Delta/\Delta}$ (n=13) ΔT_{reg} cells. Results are expressed as scatter plot and mean and represent a pool of 2 independent experiments. (**g**), In vitro suppression of T_{resp} cells by *Foxp3*$^{\Delta EGFPiCre}$*Rictor*$^{\Delta/\Delta}$ ΔT_{reg} cells carried out in the

presence of either an isotype control or anti-IL-10 mAb (n=3 per group). Results are expressed as mean ± SEM and represent 1 of 2 independent experiments. (**h**) ChIP assays for the binding of Foxo1 and control isotype to *Tbx21* and *Ifng* promoters in *Foxp3*$^{\Delta EGFPiCre}$ (n=5) and *Foxp3*$^{\Delta EGFPiCre}$*Rictor*$^{\Delta/\Delta}$ (n=13) ΔT_{reg} cells. Results are expressed as scatter plot and mean and represent a pool of 2 independent experiments. Statistical significance was determined one-way ANOVA (**e**) or two-way ANOVA (**f-h**) with Tukey's or Sidak's multiple comparisons (*P* values as indicated).

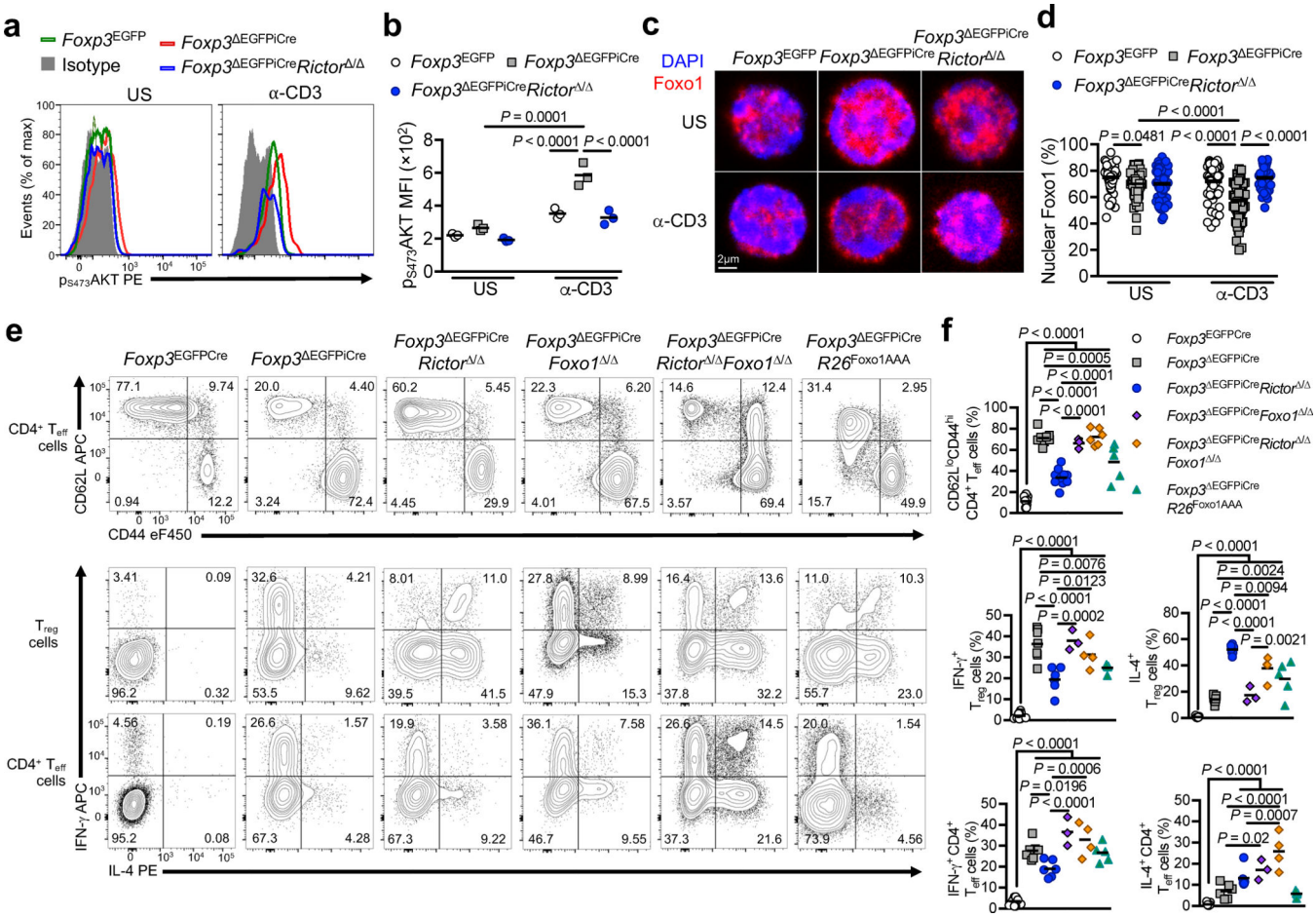

Figure 5. Contribution of AKT/Foxo1 axis to the Rictor-dependent ΔT_{reg} cell phenotype.

(**a**) Representative flow cytometric analysis and (**b**) MFI of p_{473}-AKT expression in unstimulated (US) and anti-CD3/CD28 mAb-stimulated (α-CD3+α-CD28) T_{reg} cells from *Foxp3*^{EGFPCre}, *Foxp3*$^{\Delta EGFPiCre}$, *Foxp3*$^{\Delta EGFPiCre}$*Rictor*$^{\Delta/\Delta}$ mice (n=3 per group). Results are expressed as scatter plot and mean and represent 1 of 3 independent experiments. (**c,d**) Representative confocal microscopic merge image of Foxo1 (Red) and DAPI (Blue) (**c**), and percent of nuclear Foxo1 (**d**) in unstimulated (US) or 0.1μg/mL anti-CD3 (α-CD3) stimulated T_{reg} cells from *Foxp3*^{EGFPCre} (n=53 for US, n=71 for α-CD3), *Foxp3*$^{\Delta EGFPiCre}$ (n=74 for US, n=95 for α-CD3), *Foxp3*$^{\Delta EGFPiCre}$*Rictor*$^{\Delta/\Delta}$ (n=78 for US, n=46 for α-CD3) mice. Results are expressed as scatter plot and mean and represent a pool of 2 independent experiments. (**e**) Representative flow cytometric analysis and (**f**) frequencies (scatter plot and mean) of CD62L^{lo}CD44^{hi} CD4$^+$ T_{eff} cells, and IFN-γ and IL-4 expression by CD4$^+$ T_{reg} and T_{eff} cells in spleens of *Foxp3*^{EGFPCre} (n=10), *Foxp3*$^{\Delta EGFPiCre}$ (n=7), *Foxp3*$^{\Delta EGFPiCre}$*Rictor*$^{\Delta/\Delta}$ (n=6), *Foxp3*$^{\Delta EGFPiCre}$*Foxo1*$^{\Delta/\Delta}$ (n=3), *Foxp3*$^{\Delta EGFPiCre}$*Rictor*$^{\Delta/\Delta}$*Foxo1*$^{\Delta/\Delta}$ (n=4) and *Foxp3*$^{\Delta EGFPiCre}$*R26*^{Foxo1AAA} (n=5) mice. Results represent a pool of 3 independent experiments. Statistical significance was determined one-way ANOVA with Tukey's multiple comparisons (**f**) or two-way ANOVA with Sidak's multiple comparisons (**b, d**) (*P* values as indicated).

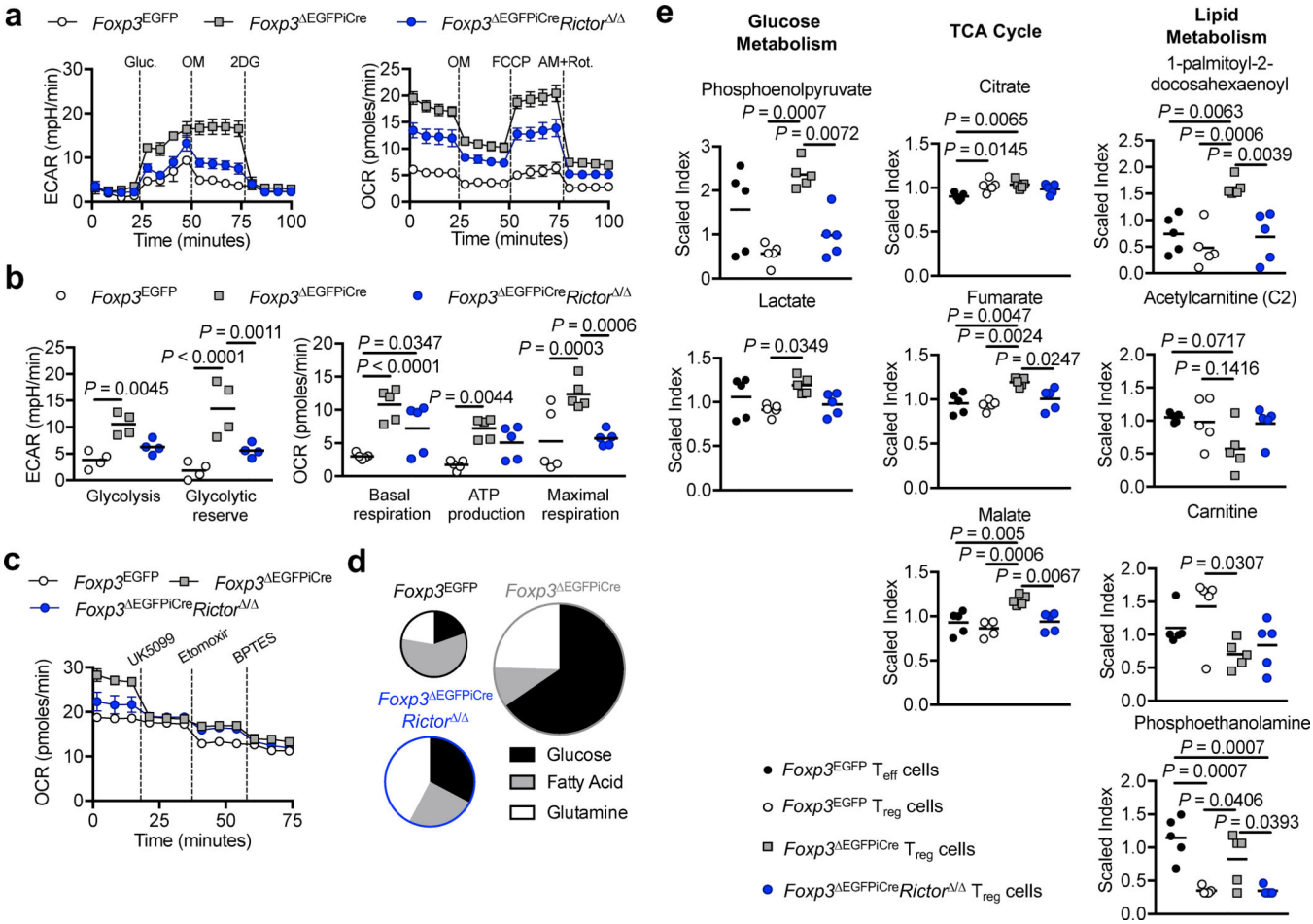

Figure 6. mTORC2 promotes aerobic glycolysis and OXPHOS in ΔT_{reg} cells.

(**a**, **b**) Extracellular acidification rate (ECAR) under glycolysis stress test conditions (n=4 per group) and Oxygen consumption rate (OCR) under mitochondrial stress test conditions (n=5 per group) of T_{reg}/ΔT_{reg} cells isolated from *Foxp3*^{EGFP}, *Foxp3*$^{\Delta EGFPiCre}$ or *Foxp3*$^{\Delta EGFPiCre}$*Rictor*$^{\Delta/\Delta}$ males (n=4 per group). Results are expressed as mean ± SEM and represent a pool of 2 independent experiments. (**c**) OCR under mitochondrial fuel test conditions (n=4 per group). Results are expressed as mean ± SEM and represent a pool of 2 independent experiments (**d**) Pie chart representation of the contribution of glucose, fatty acids and glutamine to the OXPHOS capacities in *Foxp3*^{EGFP}, *Foxp3*$^{\Delta EGFPiCre}$ and *Foxp3*$^{\Delta EGFPiCre}$*Rictor*$^{\Delta/\Delta}$ ΔT_{reg} cells. (**e**) Quantification of metabolites (expressed as scaled index) of glucose metabolism (Phosphoenolpyruvate and lactate), tricarboxylic acid (TCA) cycle (Citrate, fumarate and Malate) and lipid metabolism (Acetylcarnitine (C2), Carnitine, 1-palmitoyl-2-decosahexaenoyl and Phospho-ethanolamine) isolated from *Foxp3*^{EGFP}, *Foxp3*$^{\Delta EGFPiCre}$ and *Foxp3*$^{\Delta EGFPiCre}$*Rictor*$^{\Delta/\Delta}$ ΔT_{reg} cells (n=5 per group). Results are expressed as mean ± SEM and represent 1 experiment. Statistical significance was determined one-way ANOVA with Tukey's multiple comparisons (**e**) or two-way ANOVA with Sidak's multiple comparisons (**b**) (*P* values as indicated).

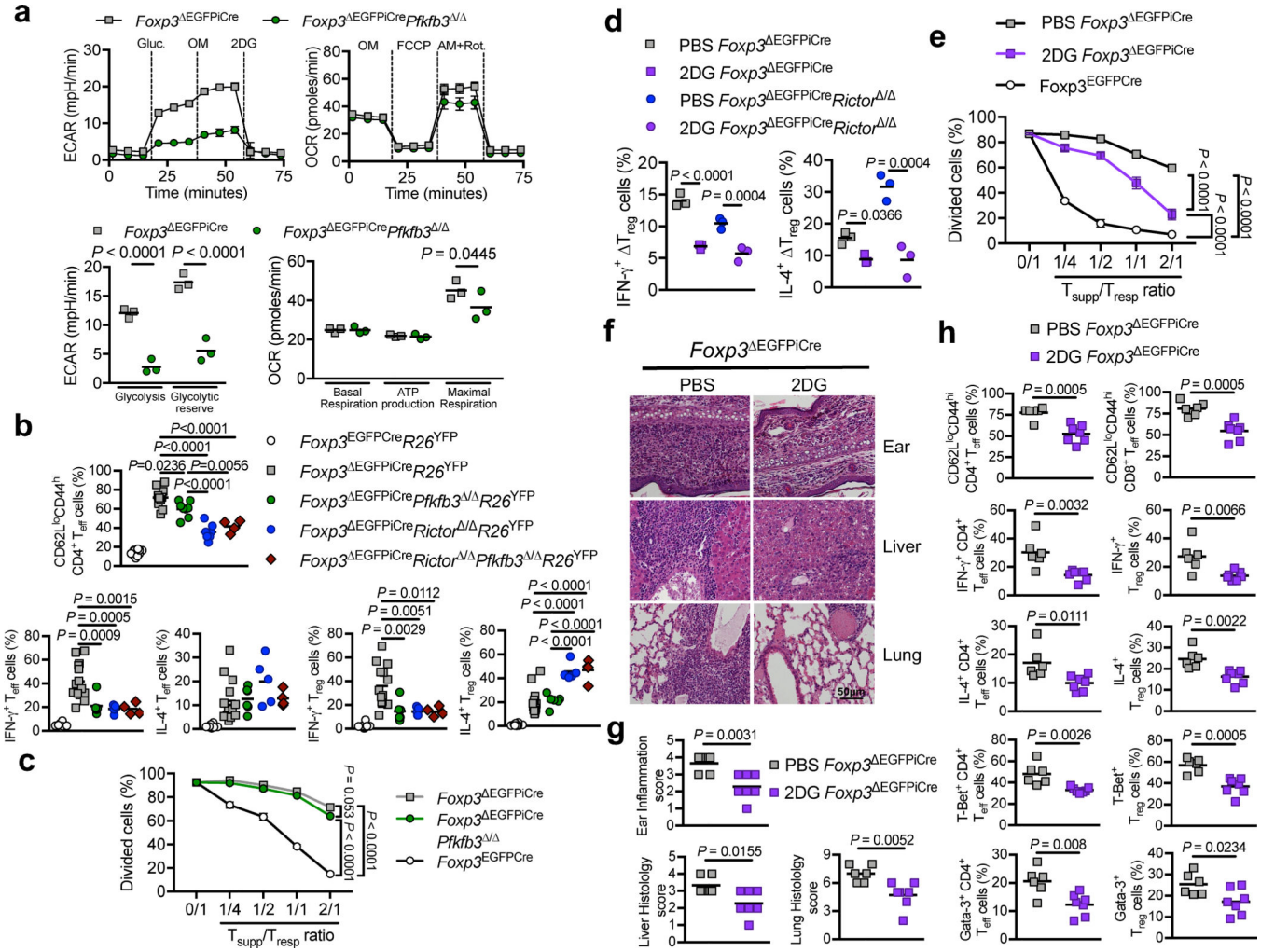

Figure 7. Blockade of glycolysis improves the scurfy phenotype of *Foxp3*$^{\Delta EGFPiCre}$ mice.

(**a**) ECAR under glycolysis stress test conditions and OCR under mitochondrial stress test conditions of ΔT_{reg} cells isolated from *Foxp3*$^{\Delta EGFPiCre}$ or *Foxp3*$^{\Delta EGFPiCre}$*Pfkfb3*$^{\Delta/\Delta}$ males (n=3 per group). Results are expressed as mean ± SEM and represent 1 of 2 independent experiments. (**b**) Frequencies of CD62L^{lo}CD44^{hi} CD4^{+} T_{eff} cells, and IFN-γ and IL-4 expression by CD4^{+} T_{reg} and T_{eff} cells in spleens of *Foxp3*^{EGFPCre}*R26*^{YFP}, *Foxp3*$^{\Delta EGFPiCre}$*R26*^{YFP}, *Foxp3*$^{\Delta EGFPiCre}$*Pfkfb3*$^{\Delta/\Delta}$*R26*^{YFP}, *Foxp3*$^{\Delta EGFPiCre}$*Rictor*$^{\Delta/\Delta}$*R26*^{YFP}, *Foxp3*$^{\Delta EGFPiCre}$*Rictor*$^{\Delta/\Delta}$*Pfkfb3*$^{\Delta/\Delta}$*R26*^{YFP} mice. Results are expressed as scatter plot and mean and represent a pool of 3 independent experiments. (**c**) In vitro suppression of CD4^{+} T_{eff} cell (T_{resp}) proliferation by *Foxp3*^{EGFPCre}, *Foxp3*$^{\Delta EGFPiCre}$ or *Foxp3*$^{\Delta EGFPiCre}$*Pfkfb3*$^{\Delta/\Delta}$ T_{reg} cells (T_{supp}) (n=3 per group). Results are expressed as mean ± SEM and represent 1 of 2 independent experiments. (**d**) Frequencies of IFN-γ^{+} and IL-4^{+} *Foxp3*$^{\Delta EGFPiCre}$*R26*^{YFP} and *Foxp3*$^{\Delta EGFPiCre}$*Rictor*$^{\Delta/\Delta}$*R26*^{YFP} sorted T_{reg} cells that were either sham treated or treated *ex-vivo* with 2-deoxyglucose (2DG) (n=3 per group). Results are expressed as scatter plot and mean and represent 1 of 2 independent experiments. (**e**) In vitro suppression of CD4^{+} T_{eff} cell (T_{resp}) proliferation by *Foxp3*$^{\Delta EGFPiCre}$ ΔT_{reg} (T_{supp}) cells that were pre-treated for 12h with either PBS (Veh ΔT_{reg}

cells) or 2DG (2DG ΔT_{reg} cells) (n=3 per group). Results are expressed as mean ± SEM and represent 1 of 2 independent experiments. (**f, g**) Representative hematoxylin and eosin-stained tissue histological sections (**f**) and tissue histological scores (**g**) of ears, livers and lungs of *Foxp3*$^{\Delta EGFPiCre}$*R26*^{YFP} mice treated with PBS (n=) or 2 μg/g 2DG (n=) every other day from day 14 to day 28. Results are expressed as scatter plot and mean and represent a pool of 2 independent experiments. (**h**) Frequencies of CD62L^{lo}CD44^{hi} CD4^{+} and CD8^{+} T_{eff} cells, IFN-γ^{+} and IL-4^{+} T_{reg} and CD4^{+} T_{eff} cells and T-Bet^{+} and Gata-3^{+} T_{reg} and CD4^{+} T_{eff} cells in *Foxp3*$^{\Delta EGFPiCre}$*R26*^{YFP} mice treated with PBS (n=6) or 2DG (n=7). Results are expressed as scatter plot and mean and represent a pool of 2 independent experiments. Statistical significance was determined unpaired t-test (**g, h**), one-way ANOVA with Tukey's multiple comparisons (**b**) or two-way ANOVA with Sidak's multiple comparisons (**a, d**) or with Tukey's multiple comparisons (**c, e**) (*P* values as indicated).

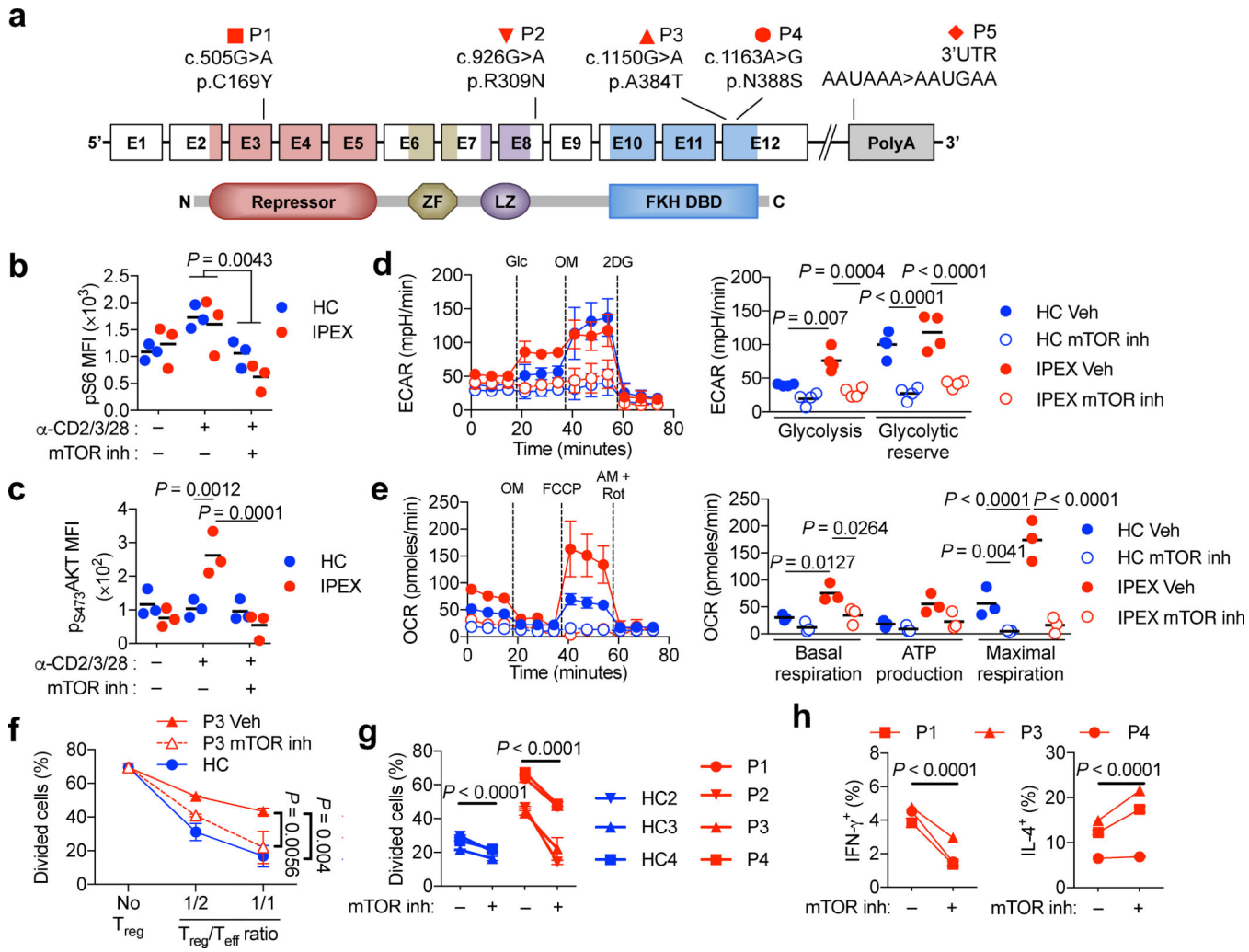

Figure 8. mTOR inhibition augments the suppressive function of human *FOXP3* mutant T_{reg} cells.

(**a**) Schematic representation of *FOXP3* illustrating the exons, the protein domains and mapped mutations of five patients. Amino acid changes are referred to by their single letter code. The N-terminal proline rich repressor domain (Repressor), zinc finger (ZF) motif, leucine zipper domain (LZ) and the forkhead DNA-binding domain (FKH DBD) are indicated. (**b,c**) Mean Fluorescence Intensity (MFI) of pS6 and p_{S473}AKT in T_{reg} cells of healthy control subjects (HC) (n=3) and IPEX patients (n=3; P1, P2, P3) stimulated with anti-CD2/CD3/CD28 mAbs (α-CD2/3/28) in the absence or presence of a competitive dual mTOR inhibitor (mTOR inh). Results are expressed as scatter plot and mean and represent 1 of 2 independent experiments. (**c**) Representative ECAR tracings (HC1 and P1), expressed as mean ± SEM. (**d**) Evaluation of glycolysis and glycolytic reserve (n=5 each for HC and IPEX groups). Results are expressed as mean ± SEM and represent a pool of 5 independent experiments. (**e**) Representative OCR tracings (HC2 and P2). Basal respiration, ATP production and maximal respiration in DMSO (Vehicle) or mTOR inhibitor (mTOR inh) treated HC and IPEX T_{reg} cells (HC n=3 and IPEX: P1, P2, P4). (**f**) In vitro suppression of third party $CD4^+$ T_{eff} cell (T_{resp}) proliferation by T_{reg} (T_{supp}) cells of a HC or an IPEX

subject (P3) that were pre-treated with vehicle or mTOR inhibitor. (**g**) Compilation of in vitro suppression assay results for HC and IPEX subjects at the ratio of 1:1 T_{reg}:T_{eff} cells without or with T_{reg} cell mTOR inhibitor pretreatment. (**h**) IFN-γ and IL-4 secretion by vehicle or mTOR inhibitor pre-treated IPEX T_{reg} cells. Statistical significance was one-way ANOVA with Tukey's multiple comparisons (**h**) or two-way ANOVA with Sidak's multiple comparisons (**b-d**) or with Tukey's multiple comparisons (**e, f**, **g**) (*P* values as indicated).